

Agentic Workflow Using RBA_{θ} for Event Prediction

Purbak Sengupta[†], Sambeet Mishra[‡], Sonal Shreya[†]

[†]Department of Electrical and Computer Engineering, Aarhus University, Denmark

E-mail: sen.purbak@gmail.com, sshreya@ece.au.dk

[‡]Department of Electrical, IT and Cybernetics, University of South-Eastern Norway, Norway

E-mail: sambeet.mishra@usn.no

Abstract—Wind power ramp events are difficult to forecast due to strong variability, multi-scale dynamics, and site-specific meteorological effects. This paper proposes an *event-first, frequency-aware* forecasting paradigm that directly predicts ramp events and reconstructs the power trajectory thereafter, rather than inferring events from dense forecasts. The framework is built on an enhanced Ramping Behaviour Analysis (RBA_{θ}) method’s event representation and progressively integrates statistical, machine-learning, and deep-learning models. Traditional forecasting models with post-hoc event extraction provides a strong interpretable baseline but exhibits limited generalisation across sites. Direct event prediction using Random Forests improves robustness over survival-based formulations, motivating fully event-aware modelling. To capture the multi-scale nature of wind ramps, we introduce an event-first deep architecture that integrates wavelet-based frequency decomposition, temporal excitation features, and adaptive feature selection. The resulting sequence models enable stable long-horizon event prediction, physically consistent trajectory reconstruction, and zero-shot transfer to previously unseen wind farms. Empirical analysis shows that ramp magnitude and duration are governed by distinct mid-frequency bands, allowing accurate signal reconstruction from sparse event forecasts. An agentic forecasting layer is proposed, in which specialised workflows are selected dynamically based on operational context. Together, the framework demonstrates that event-first, frequency-aware forecasting provides a transferable and operationally aligned alternative to trajectory-first wind-power prediction.

Index Terms—Time-series variation, uncertainty quantification, ramping behaviour analysis, renewable energy systems, event forecasting, time-series reconstruction, agentic-AI

I. INTRODUCTION

THE rapid global transition toward renewable energy has positioned wind power as a central pillar of modern electricity systems. Installed wind capacity surpassed one terawatt by 2023, with continued expansion driven by cost reductions, offshore deployment, technological maturity, and policy commitments toward low-carbon energy systems. As wind power evolves from a supplementary resource to a dominant source of electricity, its intrinsic variability arising from atmospheric processes spanning multiple temporal and spatial scales has emerged as a critical challenge for grid stability, reserve planning, and market operations.

Accurate wind power forecasting is therefore essential for operational decision-making, including scheduling, dispatch, maintenance, and energy trading. However, wind power generation exhibits pronounced nonlinearity, stochasticity, and non-stationarity, leading to large forecast uncertainty, particularly

during periods of rapid power variation. Wind power ramp events, characterized by abrupt changes in generation, are especially consequential: they account for a disproportionate share of forecast error and operational risk, yet remain among the most difficult phenomena to predict reliably [1], [2]. Improving forecasting performance during such rare but impactful events is thus a central requirement for renewable-dominated power systems.

A. Background

According to the International Renewable Energy Agency, global installed wind capacity surpassed 1 TW in 2023, contributing close to 10% of total electricity generation. As this share continues to increase, system operators face growing challenges related to variability, stability, and real-time balancing. Among the various manifestations of wind variability, ramp events represent the most critical challenge for grid operations. These events correspond to abrupt increases or decreases in power output that can trigger reserve activation, curtailment, or emergency trading, leading to substantial economic and operational consequences. Beyond financial impact, ramp events also influence turbine fatigue, grid-code compliance, and the coordination of multiple renewable resources. Empirical studies have shown that ramp events contribute disproportionately to forecasting error and grid stress [2]. At short time horizons below six hours, these effects are dominated by chaotic micro and mesoscale dynamics, limiting the predictive capability of purely physical models. Despite advances in numerical weather prediction, statistical modeling, and deep learning, most existing forecasting approaches remain fundamentally trajectory-centric. These methods optimize global error metrics such as Root mean squared error (RMSE) or Mean absolute error (MAE) over continuous time series, implicitly assuming that improved average trajectory accuracy translates into better operational performance. In practice, however, grid operators and control systems respond primarily to discrete events such as ramp onset, duration, magnitude, and regime transitions rather than to small pointwise deviations during stable periods. As a result, strong global accuracy can mask systematic failures during operationally critical intervals, particularly when forecasts misalign ramp timing or underestimate ramp intensity.

This mismatch reflects a structural limitation of trajectory-first pipelines, in which event detection is applied post hoc to

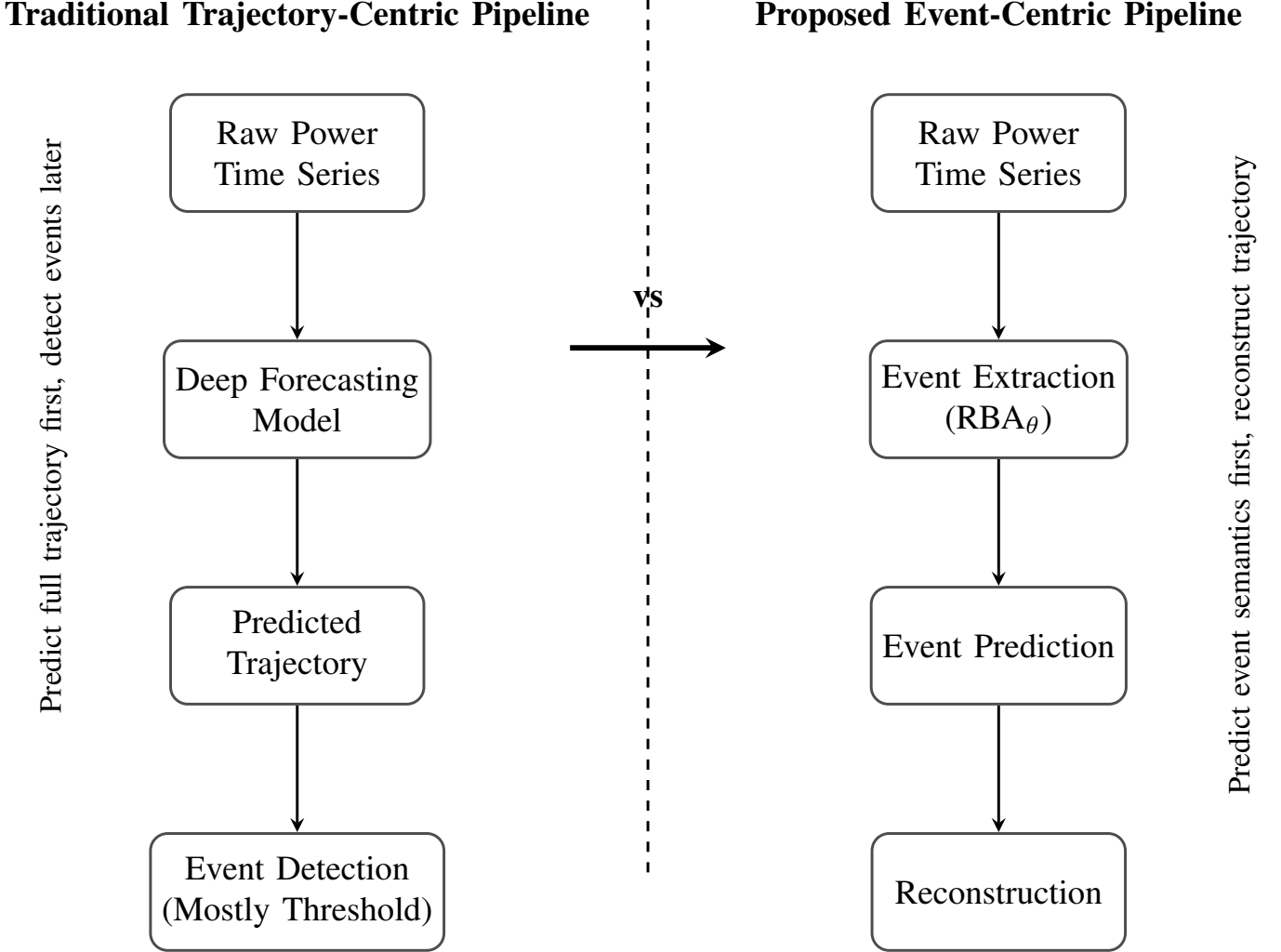


Fig. 1: Conceptual comparison between the traditional trajectory-first forecasting pipeline and the proposed event-centric paradigm. The classical approach forecasts the full time series and detects events afterward, whereas the proposed system predicts event semantics first and reconstructs the trajectory, improving interpretability, transferability, and operational relevance

predicted power trajectories. Such pipelines require uniformly accurate predictions across all timesteps, even though only a sparse subset of the signal governs operational decisions. Moreover, trajectory-based representations are highly site-specific, reducing model transferability across wind farms with differing turbine configurations, terrain, and atmospheric conditions. These limitations motivate a shift away from dense time-domain regression toward representations that explicitly encode the semantic structure of wind power dynamics.

Wind power variability is inherently multi-scale. Atmospheric processes ranging from sub-minute turbulence and wake interactions to mesoscale fronts and synoptic weather systems imprint distinct spectral signatures on power time series [3]. Empirical analyses show that ramp dynamics are concentrated within specific frequency bands, while low-frequency components govern persistence and high-frequency components largely reflect turbulence and noise. This structure suggests that ramp events are not arbitrary irregularities but organized, scale-dependent phenomena. Forecasting models

that operate solely in the time domain, without explicit multi-resolution or frequency-aware representations, are therefore intrinsically limited in their ability to capture the mechanisms underlying extreme transitions.

Recent deep learning architectures have improved nonlinear modeling capacity through convolutional, recurrent, and attention-based components. Nevertheless, most remain optimized for average predictive accuracy, leading to reduced sensitivity to rare but operationally dominant events. Predictive uncertainty typically increases during periods of rapid variation precisely when accurate forecasts are most critical and performance often degrades under distributional shifts across sites. These challenges highlight the need for forecasting paradigms that explicitly prioritize rare-event modeling, robustness, and transferability.

This work adopts an event-centric perspective in which forecasting is reframed around discrete ramp semantics rather than continuous trajectories. Building on the enhanced RBA_{θ} framework [4], which provides deterministic and physically

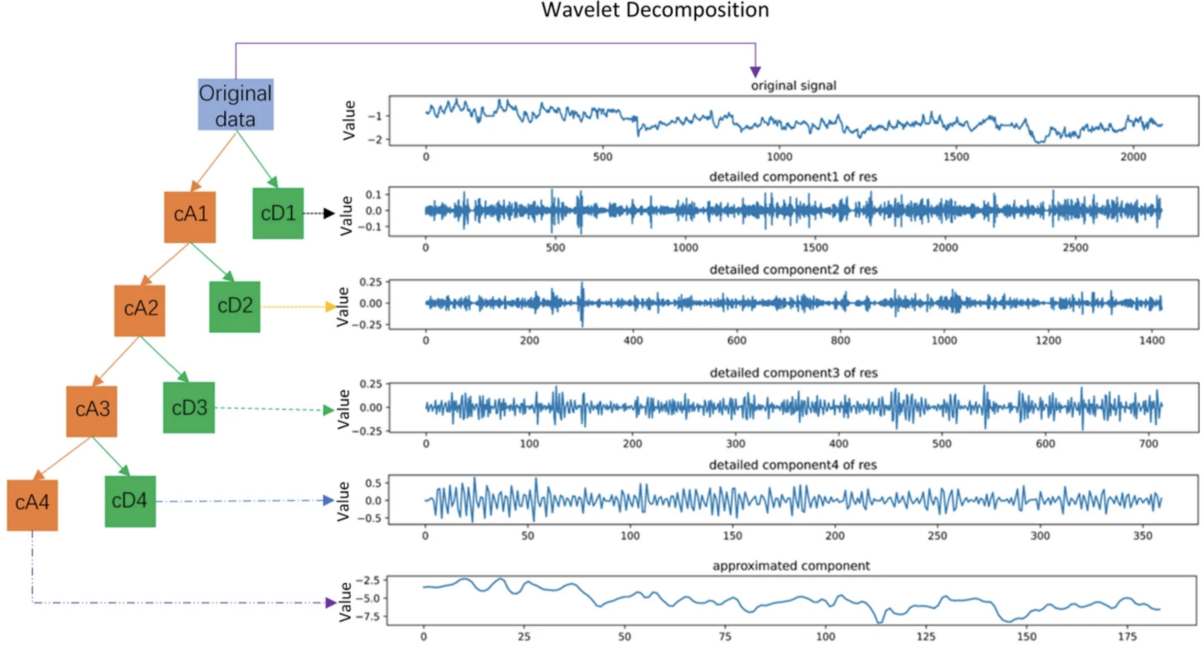


Fig. 2: Wavelet-based multi-band decomposition of the input signal, showing approximation (cA_i) and detail (cD_i) components across scales [7]

interpretable extraction of ramp events, the proposed approach treats event characteristics like onset, magnitude, duration, steepness, and type as primary predictive targets. Unlike prior studies that employ event descriptors for static thresholding based post-hoc analysis [5], the proposed paradigm inverts the conventional workflow by forecasting event structure first and reconstructing the continuous trajectory from these predictions.

Event-level representations offer two key advantages. First, they provide a naturally compressed description of wind dynamics, focusing learning capacity on the small subset of phenomena that dominate operational relevance. Second, if ramp semantics exhibit partially shared structure across sites, event-based abstractions are more likely to transfer than raw trajectories, enhancing generalization across heterogeneous wind farms. The RBA_θ mechanism yields stable and reproducible event labels, forming a consistent representation space for event-aware learning.

To capture the multi-scale nature of wind dynamics, the proposed framework integrates frequency-aware modeling via wavelet-based signal decomposition [6], [7]. Discrete wavelet transforms separate low-frequency persistence from intermediate-scale ramp dynamics and high-frequency turbulence, enabling models to focus on physically meaningful patterns while attenuating noise as shown in Fig 2. This decomposition supports more stable learning of event characteristics compared to time-domain modeling alone.

However, no single forecasting model can robustly address the diverse conditions encountered in renewable energy systems, including varying horizons, uncertainty regimes, data availability, and distributional shifts. This motivates an agentic forecasting paradigm in which multiple specialized work-

flows are coordinated through a decision layer that adapts to contextual signals such as forecast horizon, regime volatility, uncertainty level, and transfer requirements. Agentic and mixture-of-experts frameworks have demonstrated improved robustness and interpretability across complex forecasting tasks [8]–[10]. Within this paradigm, challenging periods such as ramp-dominated or uncertainty-heavy regimes can be routed to workflows explicitly designed for rare-event prediction, while simpler models handle stable conditions. By shifting predictive focus from dense trajectories to sparse, semantically meaningful events, the proposed framework aligns forecasting objectives with operational decision-making and improves robustness under uncertainty. Wind power serves as a challenging and practically relevant test case, but the proposed agentic, event-centric paradigm is broadly applicable to forecasting problems in which rare, high-impact events dominate operational risk.

Ramp events are commonly defined as intervals during which wind power changes exceed a specified threshold within a fixed time window. Their primary descriptors include amplitude, duration, rate of change, direction, onset time etc [5]. The RBA_θ framework formalized this concept through slope-angle analysis of power trajectories, enabling systematic extraction of event-level features such as duration, intensity, and balance. Their analysis revealed that only a small fraction of samples typically correspond to ramp conditions, yet these intervals account for majority of the total power variance, highlighting their operational relevance.

Subsequent work extended this framework by introducing adaptive thresholding, Bayesian tuning, and Monte Carlo evaluation to handle non-stationary environments and quantify uncertainty [4]. This enhanced RBA_θ formulation bridged de-

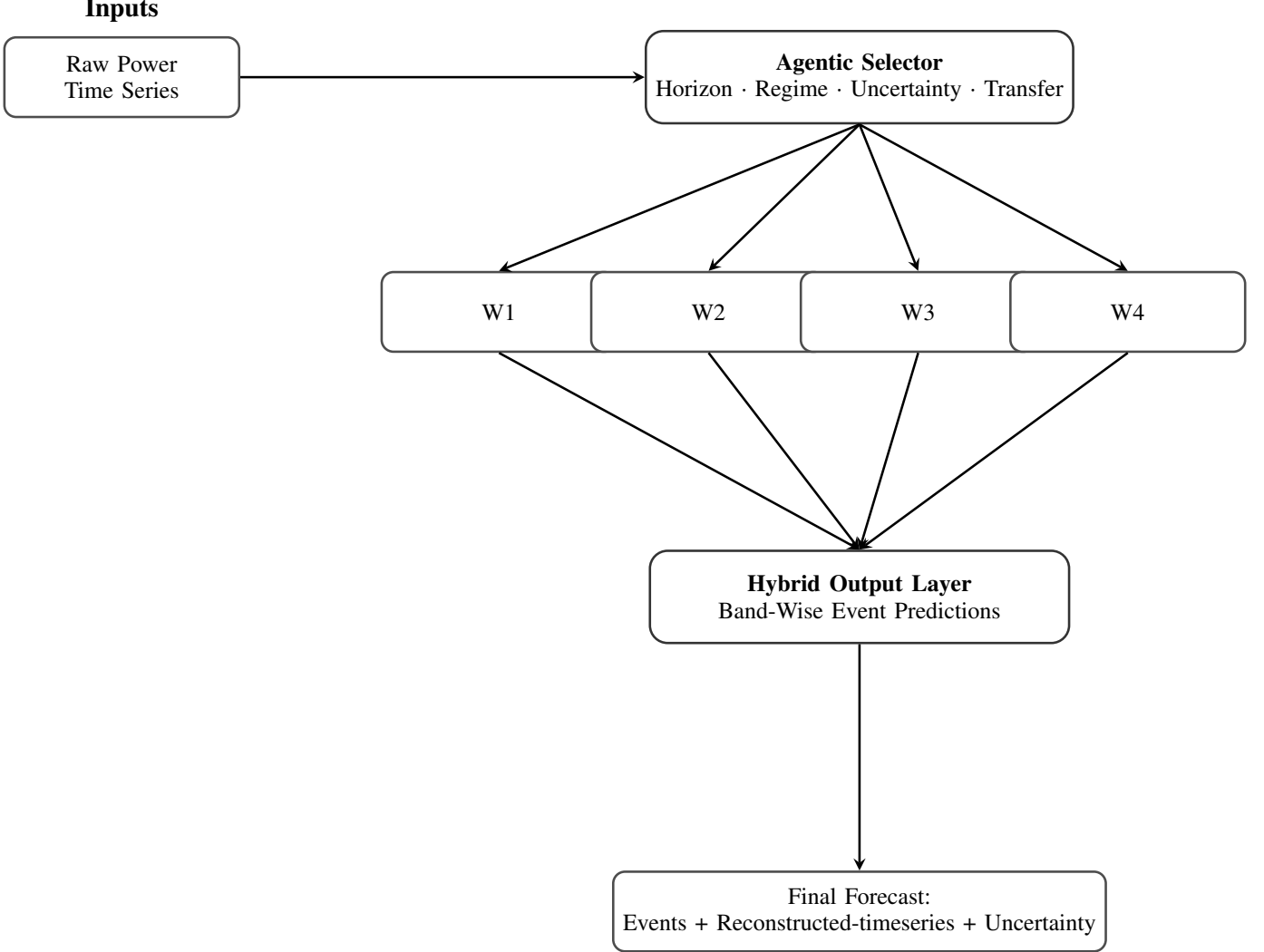


Fig. 3: Conceptual overview of the agentic forecasting system developed where $\{W_x\}$ are designed workflows

terministic event detection with statistical reasoning, enabling more robust identification of ramps under varying atmospheric regimes. Nevertheless, predicting ramp events remains considerably more challenging than detecting them. The nonlinear relationship between wind speed and power output, together with mechanical lag, turbulence, and sensor noise, amplifies small input errors into large output deviations, particularly during rapid transitions.

A broad range of approaches has been proposed to address ramp detection and forecasting. Early threshold-based segmentation methods offer transparency and low computational cost but require manual tuning and exhibit limited transferability across sites. More recent studies combine signal decomposition techniques with deep learning architectures. Hybrid models incorporating wavelet transforms, Convolution Neural Networks, LSTMs, attention mechanisms, or variational decomposition have demonstrated improvements in ramp detection and short-horizon forecasting [11]–[13]. Similarly, [14] found that while LSTM-RNN models achieved high accuracy on non-ramp intervals, they frequently underperformed during abrupt ramps, often missing extreme high readings and overfitting

on stable data. This reinforces that ramp prediction operates under a distinct stochastic regime, where model assumptions suited for average dynamics break down in rare, high-impact deviations. In parallel, meteorological ensemble models such as NOAA HRRR have improved physical consistency but continue to exhibit substantial timing and amplitude errors at local scales [15]. Review studies consistently report persistent challenges related to data imbalance, threshold sensitivity, and inadequate uncertainty representation [16], [17]. Likewise, [18] shows that standard classification models trained on heavily imbalanced wind-power data can achieve high aggregate accuracy while exhibiting weak sensitivity to rare, high-impact ramp events. Even with imbalance-mitigation strategies, performance gains on extreme events remain limited, indicating that stochastic volatility and class skew impose structural constraints on generalisation. As a result, models optimised for average behaviour tend to underperform precisely in operationally critical scenarios.

Despite this progress, existing approaches remain fragmented across detection, forecasting, and uncertainty modeling. Event extraction is often treated as a preprocessing step

rather than a co-evolving component of the forecasting system. This separation limits the ability to exploit shared structure between ramp onset, evolution, and dissipation, and motivates a transition toward integrated, event-aware forecasting systems.

B. Knowledge Gap and Motivation

Although wind ramp research has advanced substantially, several fundamental gaps persist in event-level forecasting. First, there is no unified formulation of the ramp prediction problem. Existing studies variously frame ramps as binary classification tasks, magnitude regression problems, or two-stage detect-then-predict pipelines [12], [19]. These formulations rely on differing definitions, thresholds, and evaluation metrics, which complicates comparison across datasets and masks true generalization capability. Reported improvements are often dataset-specific and difficult to transfer across sites or regimes.

Second, ramp events occur infrequently, typically representing fewer than 5% of samples [15]. This severe imbalance biases learning toward smooth operating conditions and degrades performance during rare but critical extremes. Even advanced deep architectures tend to minimize average error while misrepresenting ramp timing and magnitude, achieving low RMSE yet poor event-level reliability. This limitation reflects a structural mismatch between trajectory-based optimization objectives and event-driven operational needs.

Third, evaluation practices remain largely trajectory-centric. Metrics such as RMSE, MAE, and CRPS quantify average accuracy but fail to capture event timing, duration overlap, or directional correctness. Event-centric measures, including onset-time error, interval overlap, and event-wise precision or recall, are seldom reported. Moreover, probabilistic calibration diagnostics are rarely extended to discrete events, leaving the reliability of ramp forecasts insufficiently assessed.

Fourth, most forecasting pipelines are structurally rigid. Single-architecture models are applied uniformly across sites and regimes despite strong evidence that wind dynamics vary with terrain, atmospheric stability, and seasonal effects [20], [21]. Few systems diagnose signal characteristics such as variance, entropy, or spectral composition and adapt their modeling strategy accordingly. The absence of autonomous workflow selection limits robustness under domain shift and constrains scalability.

Fifth, uncertainty is typically treated as a secondary output derived from ensemble spread or residual analysis. While probabilistic forecasting of continuous trajectories has matured, uncertainty at the event level remains largely unexplored. Existing methods rarely quantify confidence in event occurrence, timing, magnitude, or duration, despite the central role of such information in risk-aware grid operation [21], [22]. The gap between trajectory-level uncertainty and event-level reliability remains unresolved.

Finally, interpretability and automation remain underdeveloped. Many deep models obscure physically meaningful descriptors such as slope, duration, and symmetry that are central to the RBA_θ methodology. At the same time, practical deployment is hindered by manual threshold tuning,

site-specific retraining, and ad hoc preprocessing. End-to-end systems capable of autonomous execution and interpretable, event-aware outputs remain scarce. The emerging paradigm of agentic systems which are capable of introspection, self-configuration, and dynamic pipeline assembly promises transformative efficiency. LLM-based market agents have already shown practical autonomy in decision-intensive electricity markets, where a bidding-behavior agent and a sentiment agent improved 5-minute day-ahead spike and price predictions [23]. Translating this approach to physical time-series prediction together with other gaps collectively motivate a shift toward an integrated, agentic, event-centric forecasting paradigm that unifies detection, prediction, uncertainty quantification, and adaptive workflow selection. Within this context, the present work addresses the research questions presented in table I. Together, these questions articulate the need for forecasting systems that are adaptive, interpretable, and uncertainty-aware, aligning predictive objectives with the operational realities of renewable-dominated power systems.

II. METHODOLOGIES

This section presents the methodological framework developed in this work. The overall system is organized as a set of complementary forecasting workflows, each representing a distinct modeling philosophy, and coordinated by an agentic selector that adapts to data characteristics and operational regimes. To establish a reliable reference point, we first introduce a transparent, trajectory-first baseline that reflects prevailing industrial practice. Subsequent approaches progressively incorporate event-centric learning, frequency-aware modeling, and adaptive workflow selection.

A. Approach 1: Trajectory-First Forecasting with Post-hoc Event Extraction

The first methodological component establishes an interpretable and fully reproducible baseline that reflects prevailing operational practice in wind power forecasting. The workflow follows a two-stage paradigm in which the wind-power trajectory is first forecast at the signal level and ramp-related events are subsequently extracted from the predicted series. Specifically, a Seasonal AutoRegressive Integrated Moving Average model with exogenous variables (SARIMAX) [24] is used to generate short-term forecasts, after which ramp and stationary periods are identified using the enhanced RBA_θ framework.

This decoupled design provides a transparent control condition against which more advanced hybrid and agentic methods can be evaluated. Errors introduced during forecasting and errors arising from event extraction remain separable, enabling direct attribution of performance degradation to either the trajectory model or the event logic. Such diagnostic clarity is essential for the later agentic selector, which must determine whether failures stem from inadequate signal modeling or from event-level interpretation.

Formally, given a historical wind-power series $W(t)$ and exogenous meteorological covariates $X(t)$ observed over a training interval, the forecaster produces a predicted trajectory

TABLE I: Research questions guiding the design and evaluation of the proposed agentic, event-centric forecasting framework

RQ	Research Question
RQ1	Can a modular, agentic forecasting system be designed to select and combine modeling workflows based on the statistical and spectral characteristics of the input signal, instead of relying on a single fixed architecture?
RQ2	How can ramp detection and forecasting be jointly optimized to predict event occurrence together with duration, magnitude, and direction within a unified learning framework?
RQ3	How can uncertainty be modeled, quantified, and evaluated at the event level, including confidence in the timing, magnitude, and duration of predicted ramp events?
RQ4	What benefits arise from transitioning from trajectory-first forecasting to an event-first, frequency-aware modeling approach with respect to accuracy, robustness, reconstruction fidelity, and computational efficiency?
RQ5	How robust is an agentic, event-centric forecasting system across sites, temporal resolutions, and data regimes, and to what extent can event semantics support generalization beyond wind power time series?

$\widehat{W}(t)$ over the test horizon. Event predictions are obtained by applying RBA_θ directly to the forecast,

$$E_{\text{pred}} = \text{RBA}_\theta(\widehat{W}(t)), \quad (1)$$

while ground-truth events E_{act} are extracted from the observed series using the same event logic. This symmetry enables event-level evaluation using overlap-based precision, recall, F1-score, and intersection-over-union (IoU).

For computational efficiency, the SARIMAX configuration adopted in this work employs no-differencing order $(p, d, q) = (1, 0, 1)$ and turned-off seasonal order $(P, D, Q, m) = (0, 0, 0, 0)$. The model can be written as

$$y_t = c + \phi_1 y_{t-1} + \theta_1 \varepsilon_{t-1} + \beta^\top X_t + \varepsilon_t, \quad (2)$$

where y_t denotes the raw wind-power series, ε_t is white noise, and X_t represents the selected exogenous variables. We compensate the omission of seasonal order through weather feature engineering and RBA_θ event descriptors. This formulation captures linear temporal dependencies, daily periodicity, and meteorological forcing while preserving coefficient interpretability.

Event extraction is performed using slope-based ramp logic central to RBA_θ . Scale-normalized power gradients are computed using a symmetric difference,

$$\nabla P(t) = \frac{P(t + \Delta t) - P(t - \Delta t)}{2 \Delta t P_{\text{rated}}}, \quad (3)$$

where P_{rated} is the turbine rated power. A ramp event is declared when the gradient magnitude exceeds an adaptive threshold $\tau(t)$ for a minimum duration,

$$|\nabla P(t)| > \tau(t), \quad \text{duration} > T_{\text{min}}. \quad (4)$$

To accommodate non-stationary operating conditions, adaptive thresholds are employed. A statistically motivated rule defines

$$\tau_{\text{stat}}(t) = \mu_w(t) + k_\sigma \sigma_w(t), \quad (5)$$

where $\mu_w(t)$ and $\sigma_w(t)$ denote rolling statistics of the signal or its slope proxy. Stationary intervals are identified using complementary constraints on rolling slope, variance, and range, which substantially reduce false positives in low-variability regimes. Each detected event is characterized by onset time, duration, magnitude, direction, and auxiliary descriptors such as slope variance and symmetry [5].

This baseline reflects common industrial forecasting pipelines, where signal-level predictions are produced upstream and interpreted downstream in terms of operationally meaningful events. Its statistical transparency, auditability, and explicit uncertainty propagation make it a suitable benchmark for evaluating the benefits of event-centric and agentic forecasting strategies introduced in subsequent sections.

B. Approach 2: Direct Event Prediction Guided by RBA_θ

While the trajectory-first baseline provides transparency and diagnostic clarity, it inherently depends on accurate signal-level forecasting and therefore propagates trajectory uncertainty directly into event estimates. To address this limitation, the second methodological component adopts an event-first perspective in which ramp events are predicted directly, without explicitly forecasting the full power trajectory. This approach leverages the semantic structure exposed by RBA_θ and treats events as the primary prediction target rather than as post-hoc interpretations of a continuous signal.

The key premise of this approach is that many operational decisions depend on the timing, type, and persistence of events rather than on pointwise power values. By shifting the modeling focus from dense trajectories to discrete event semantics, this method reduces sensitivity to short-term signal noise and aligns more closely with the objectives of event-aware grid operation. It also establishes a complementary workflow that can be selected by the agentic controller when trajectory forecasting is unreliable, for instance under high turbulence or weak seasonality.

An initial attempt to realize this paradigm employed Survival Analysis, motivated by the natural correspondence between ramp forecasting and time-to-event modeling. Using Accelerated Failure Time formulations, the time until the next significant or stationary event was modeled as a function of RBA_θ -derived descriptors such as event duration, magnitude, slope angle, and local variability. Despite its conceptual appeal, this approach exhibited limited empirical performance. Practical difficulties included sensitivity to sparse and irregular event spacing, instability of parametric assumptions, and frequent fallback to non-parametric estimators. These results indicated that classical survival models were too restrictive to capture the nonlinear and highly variable dynamics of wind-power ramps.

This observation motivated a transition to a more flexible yet still interpretable learning framework based on Random Forest

TABLE II: Key hyperparameters used in the RBA_θ -guided Random Forest event prediction workflow

Parameter	Symbol	Description
Significant-event threshold multiplier	τ_{sig}	Multiplier controlling sensitivity of RBA_θ for detecting significant ramp events.
Stationary-event threshold multiplier	τ_{stat}	Threshold factor governing detection of stationary regimes in RBA_θ .
Minimum event duration	d_{min}	Minimum temporal length required for a detected event to be retained.
Event-detection probability threshold	τ_{event}	Probability cutoff converting pointwise RF scores into event occurrence labels.
Minimum inter-event gap	gap_{min}	Minimum temporal separation enforced between consecutive events.
Temporal matching tolerance	δ	Allowed deviation when matching predicted events to ground-truth intervals.
Number of trees (event detection)	B_1	Number of trees in the Random Forest used for event detection.
Maximum tree depth (event detection)	D_1	Maximum depth of trees in the detection-stage Random Forest.
Number of trees (event classification)	B_2	Number of trees in the Random Forest used for event-type classification.

classifiers. The adopted architecture decomposes direct event prediction into two sequential classification tasks. The first stage determines whether a significant event is occurring at a given time step, while the second stage assigns the significant event category, distinguishing between up and down ramps. This separation allows the model to learn onset dynamics and event semantics independently, without imposing distributional assumptions on event timing.

Let $x_t \in \mathbb{R}^d$ denote the feature vector at time t , composed of RBA_θ structural descriptors, meteorological covariates, and temporal encodings. Event occurrence is modeled as a probabilistic mapping

$$\hat{y}_t = f(x_t) = \Pr(y_t = 1 \mid x_t), \quad (6)$$

where $y_t \in \{0, 1\}$ indicates the presence of an event. Conditioned on $\hat{y}_t = 1$ i.e., for significant event time-steps, the type is predicted via

$$\hat{p}_t^{\text{sig}} = g(x_t) = \Pr(c_t = \text{significant} \mid y_t = 1, x_t), \quad (7)$$

with $c_t \in \{\text{significant, stationary}\}$. Both mappings are implemented using Random Forest ensembles trained on labels obtained from ground-truth RBA_θ segmentation. The hyperparameter used for this approach is described in table II.

The detection stage is optimized using binary cross-entropy,

$$\mathcal{L}_{\text{det}} = -\frac{1}{N} \sum_t [y_t \log \hat{y}_t + (1 - y_t) \log(1 - \hat{y}_t)], \quad (8)$$

while the type classifier minimizes an analogous loss over significant event points only. In the Random Forest setting, both objectives are approximated implicitly through impurity reduction, with the Gini index

$$G(S) = 1 - \sum_k p_k^2 \quad (9)$$

used to guide split selection, where p_k denotes the class proportion within node S . Feature importance is computed as the average impurity decrease across trees, preserving interpretability of RBA_θ -derived descriptors.

Pointwise predictions are subsequently aggregated into contiguous event intervals by thresholding \hat{y}_t and enforcing temporal continuity. Each predicted event is represented by its onset time, termination time, and class label, and matched to ground truth using a fixed temporal tolerance on boundaries. Event-level Precision, Recall, and F1-score are computed based on these matched intervals.

Although this Random Forest formulation is not the final architecture of the proposed system, it plays a critical role within the overall framework. It empirically demonstrates that direct event prediction is both feasible and substantially more effective than classical time-to-event modeling. Moreover, it provides a robust, interpretable workflow that can be autonomously selected by the agentic controller when signal-level forecasting is unreliable. As such, this approach constitutes a necessary intermediate step toward the fully event-centric, uncertainty-aware hybrid models introduced in the subsequent methodologies.

C. Approach 3: Event-Aware Predictive Modelling via RBA_θ -LSTM

While Approach 1 follows a trajectory-first paradigm and Approach 2 demonstrates that direct event prediction is feasible without explicit signal forecasting, both remain limited in their ability to model *event morphology as a structured temporal object*. In particular, pointwise classification does not capture the coupled evolution of event onset, magnitude, duration, and uncertainty across time. Approach 3 introduces a fully event-aware, sequence-to-sequence predictive framework that transforms the enhanced RBA_θ representation from a retrospective detector into a forward-looking model that anticipates future event semantics. Rather than forecasting the full signal or predicting isolated labels, the proposed model directly predicts the temporal evolution of event attributes and reconstructs the underlying trajectory only as a derived quantity when required.

1) *Design rationale*: The final architecture is shaped by three empirical observations. First, event occurrence and event severity are governed by distinct temporal dynamics and cannot be learned reliably from a single fixed-scale representation. Second, wind-power events exhibit strong temporal clustering, requiring explicit modelling of event-to-event dependence. Third, different frequency components of the signal encode fundamentally different physical processes, and forcing a single predictor to represent all scales leads to systematic underfitting. These observations motivate a design that combines explicit multi-resolution signal decomposition,

causal modelling of event excitation, and frequency-aware prediction heads, while retaining the interpretability and physical grounding of RBA_θ .

2) *Final event-aware architecture*: The final workflow integrates five tightly-coupled modules: enhanced RBA_θ event semantics, DWT-based multi-resolution decomposition, stratified bandit feature selection, a Hawkes layer modelling event clustering, and an encoder LSTM with frequency-aware prediction heads. After prediction of events, those are converted back into a reconstructed time series using the reconstruction method discussed in II-C3. A schematic overview of the final pipeline is shown in Fig. 4.

a) *Multi-resolution targets and inputs*: Let $P(t)$ denote the normalised power signal. A level-4 DWT decomposes $P(t)$ into an approximation component and detail components namely `Details_1` (D1), `Details_2` (D2), `Details_3` (D4), and `Details_4` (D4). Enhanced RBA_θ is applied on each decomposed bands to obtain event-wise targets (onset, duration, magnitude, type) and timestep-level feature channels (event state, time-since-last-event, band statistics). These channels are concatenated into a multivariate sequence which the LSTM consumes over a fixed window length S to predict event attributes over one or more horizons \mathcal{H} .

b) *Horizon-aware stratified feature selection*: The expanded multi-resolution representation yields a large and heterogeneous feature space. To retain interpretability while avoiding over-parameterisation, the model employs a horizon-aware, stratified multi-armed bandit (MAB) feature-selection mechanism based on Thompson sampling. Features are grouped into six semantic categories (RBA_θ , DWT, weather, power, temporal, and nonlinear), each assigned a guaranteed quota to preserve domain balance.

Let $X \in \mathbb{R}^{N \times F}$ denote the engineered feature matrix and $Y \in \{0, 1\}^{N \times |\mathcal{H}|}$ the horizon-specific event labels. Each feature f is associated with a Beta posterior

$$\theta_f \sim \text{Beta}(\alpha_f, \beta_f), \quad (10)$$

which represents the probability that feature f contributes positively to event prediction. At each bandit round and for each prediction horizon, candidate subsets are sampled within each category according to (10) and evaluated using a lightweight Random Forest trained on temporally consistent splits.

The reward is defined as a horizon-balanced F1 score, and posterior parameters are updated as

$$(\alpha_f, \beta_f) \leftarrow \begin{cases} (\alpha_f + 3, \beta_f), & \text{high reward,} \\ (\alpha_f + 1, \beta_f), & \text{moderate reward,} \\ (\alpha_f, \beta_f + 1), & \text{otherwise,} \end{cases} \quad (11)$$

encouraging exploration while progressively favouring features with stable predictive utility. After R_{mab} rounds, features are ranked by expected reward $\mathbb{E}[\theta_f]$ and the top candidates per category are retained.

This procedure yields a compact feature set (approximately 75 predictors) that is horizon-sensitive, category-balanced, and dominated by physically meaningful ramp-scale components, particularly the D3 wavelet band.

c) *Hawkes intensity as an auxiliary causal prior*: To account for bursty event arrivals, the model includes a Hawkes intensity term that increases event likelihood after recent events. Using detected event times $\{t_i\}$, the intensity is

$$\lambda(t) = \mu + \sum_{t_i < t} \alpha e^{-\beta(t-t_i)}, \quad (12)$$

where μ is a baseline rate and α, β control excitation strength and decay. The resulting intensity features are appended to the LSTM inputs, improving calibration of event occurrence under clustered regimes.

d) *LSTM encoder & Frequency-aware prediction heads*: Hawkes causality features concatenated with other input features are passed through two-stack LSTM encoders that produces a final latent representation of the input sequence z . Rather than a single output head, the latent sequence embedding is mapped to band-conditioned heads. This avoids forcing one output map to represent slow trend structure and ramp-scale dynamics simultaneously. In practice, the model predicts global event tasks (occurrence, type, time-to-event) and band-specific attributes (magnitude and duration contributions per band), then fuses these predictions into a final event tuple and, optionally, a reconstructed time series.

e) *Multi-task objective with band-aware weighting*: The event-aware model is trained using a joint multi-task objective that combines classification and regression losses across global event attributes and frequency-specific components. This formulation explicitly prioritises ramp-relevant structure while remaining robust to heavy-tailed wind-power dynamics.

Let z denote the latent representation produced by the LSTM encoder. Global event attributes are predicted as

$$p_{\text{occ}} = \sigma(W_{\text{occ}}z), \quad (13)$$

$$p_{\text{type}} = \text{softmax}(W_{\text{type}}z), \quad (14)$$

$$t_{\text{pred}} = \text{ReLU}(W_{\text{time}}z), \quad (15)$$

corresponding to event occurrence, event type, and time-to-event, respectively. For each DWT band $b \in \{\text{approx}, D4, D3, D2, D1\}$, band-conditioned heads predict magnitude and duration contributions:

$$m_b = W_{\text{mag}}^{(b)}z, \quad (16)$$

$$d_b = \text{ReLU}(W_{\text{dur}}^{(b)}z), \quad (17)$$

where the frequency-aware parameterisation prevents slowly-varying, large-amplitude components from dominating ramp-scale dynamics. To reflect the differing physical importance of each band, fixed importance weights are assigned as

$$w_{\text{approx}} = 1.5, \quad w_{d4} = 4.0, \quad w_{d3} = 2.5,$$

$$w_{d2} = 0.5, \quad w_{d1} = 0.5.$$

Magnitude and duration are optimised using a Huber loss $L_{\text{Huber}}(\cdot)$ with $\delta = 1$, yielding

$$L_{\text{mag}} = \frac{\sum_b w_b L_{\text{Huber}}(m_b, m_b^*)}{\sum_b w_b}, \quad (18)$$

$$L_{\text{dur}} = \frac{\sum_b w_b L_{\text{Huber}}(d_b, d_b^*)}{\sum_b w_b}. \quad (19)$$

where m_b , d_b are predictions and m_b^* , d_b^* are ground truths. Huber loss is employed to ensure robustness to extreme ramps and abrupt duration variations, which are common in wind-power signals. The global classification and timing objectives are defined as

$$L_{\text{occ}} = \text{BCE}(p_{\text{occ}}, y_{\text{occ}}), \quad (20)$$

$$L_{\text{type}} = \text{CE}(p_{\text{type}}, y_{\text{type}}), \quad (21)$$

$$L_{\text{time}} = L_{\text{Huber}}(t_{\text{pred}}, t^*), \quad (22)$$

The final training objective is a weighted sum of all components:

$$L_{\text{total}} = 2.0 L_{\text{occ}} + 1.2 L_{\text{type}} + 1.0 L_{\text{time}} + 2.0 L_{\text{mag}} + 2.0 L_{\text{dur}}. \quad (23)$$

This weighting emphasises accurate event detection and event-property estimation while maintaining balanced contributions across frequency bands.

3) *Event-Guided Time-Series Reconstruction*: The final component of Approach 3 is a reconstruction module that converts predicted event semantics back into a physically plausible wind-power trajectory. Reconstruction is not treated as a post-processing convenience, but as a structural validation of whether the model has learned meaningful event dynamics rather than merely discriminative patterns. In particular, high event-detection accuracy without coherent reconstruction would indicate that the model detects changes without understanding their magnitude, duration, or temporal context.

The central challenge arises from the event-centric formulation itself. Events are discrete objects, whereas the target signal is continuous. Naive reconstruction from predicted events alone creates large gaps between consecutive events, since the model has no explicit representation of inter-event dynamics. This problem is exacerbated in the multi-resolution setting, where event extraction across wavelet bands discards fine-grained coefficient information if not handled carefully.

To address this, reconstruction is formulated as a *hybrid event-trend fusion* problem that combines predicted event attributes with a slowly varying baseline estimated from the approximation band. Crucially, no future ground-truth information is used at inference time.

a) *Baseline decomposition*: Let the predicted outputs of the event-aware model consist of event-level predictions for significant and stationary events (onset, duration, magnitude, type), and band-conditioned magnitude and duration estimates for the detail bands (primarily D_3 and D_4 , which dominate ramp dynamics). The approximation band is treated separately, as it represents the low-frequency trend of the signal.

b) *Approximation-band handling*: Rather than reconstructing the approximation component solely from predicted events (which proved unstable), the method leverages the slow temporal evolution of the approximation band. At inference time, the model produces a predicted approximation trajectory $\hat{A}_4(t)$. In parallel, a reference approximation $\tilde{A}_4(t)$ is obtained by propagating the most recent past approximation coefficients forward, which is feasible because A_4 varies slowly relative to the prediction horizons. A trend-consistency check is then performed. Both $\hat{A}_4(t)$ and $\tilde{A}_4(t)$ are smoothed using a wide

Algorithm 1 Event-Aware Forecasting with RBA_θ -LSTM

Require: Time series $P(t)$, meteorological covariates $W(t)$, wavelet ψ , decomposition level L , prediction horizon h , sequence length S .

Ensure: Predicted events $\hat{\mathcal{E}}$ and reconstructed signal $\hat{P}(t)$.

```

1: procedure EVENTAWAREFORECAST( $P(t), W(t)$ )
2:   Decompose  $P(t)$  using DWT:
    $(A_4, D_4, D_3, D_2, D_1) \leftarrow \text{DWT}(P, \psi, L)$ 
3:   for each band  $b \in \{A_4, D_4, D_3, D_2, D_1\}$  do
4:      $\mathcal{E}_b \leftarrow \text{RBA}_\theta(b)$ 
5:   end for
6:    $\mathcal{E} \leftarrow \text{FUSEEVENTS}(\{\mathcal{E}_b\})$ 
7:    $F \leftarrow \text{FEATUREENGINEERING}(P, W, \mathcal{E})$ 
8:    $F^* \leftarrow \text{BANDITSELECT}(F)$ 
9:    $\lambda(t) \leftarrow \text{HAWKESINTENSITY}(\mathcal{E})$ 
10:   $Z \leftarrow \text{LSTMENCODE}(F^*, \lambda)$ 
11:   $\hat{\mathcal{E}} \leftarrow \text{PREDICTEVENTS}(Z)$ 
12:   $\hat{P}(t) \leftarrow \text{RECONSTRUCT}(\hat{\mathcal{E}}, A_4)$ 
13:  return  $\hat{\mathcal{E}}, \hat{P}(t)$ 
14: end procedure

```

Gaussian filter to extract their low-frequency trend components. If the correlation between the predicted and propagated trends exceeds a fixed threshold, the predicted approximation is retained. Otherwise, the propagated approximation is used as the baseline. This mechanism prevents the reconstruction from drifting when the model fails to learn long-term trends, while still allowing learned trends to dominate when they are reliable.

c) *Event-driven detail reconstruction*: High-frequency structure is reconstructed exclusively from predicted events. Only the detail bands that carry ramp-relevant dynamics (typically D_3 and D_4) are used. For each predicted event, its magnitude and duration are mapped to a time-localised contribution in the corresponding band. Between consecutive events, values are interpolated smoothly to close temporal gaps, ensuring continuity without introducing artificial oscillations. Stationary events constrain slope and variance in their intervals, preventing spurious ramps in low-activity regions. Lower-energy noise-dominated bands (D_1 and D_2) are not reconstructed from predictions; their contribution is suppressed to avoid amplifying uncertainty.

d) *Boundary anchoring and smoothing*: Even with correct band fusion, small baseline offsets at the temporal boundaries can propagate across the reconstructed signal. To prevent this, the reconstruction is anchored at the sequence boundaries using a short transition window. Within this window, reconstructed values are smoothly blended with boundary reference values to eliminate discontinuities while preserving interior predictions. This produces a temporally coherent signal without sharp entry or exit artifacts.

e) *Final reconstruction*: The complete reconstructed signal is obtained by summing the selected approximation baseline with the reconstructed detail-band components and applying the inverse discrete wavelet transform. The result is a continuous trajectory whose large-scale trend is stable, whose

ramp structure is shaped by predicted events, and whose inter-event regions are filled in a physically consistent manner. This reconstruction strategy closes the loop of the event-aware forecasting pipeline. It ensures that predicted events correspond to a realizable time series, thereby validating that the model has learned event morphology and temporal dynamics rather than relying on classification shortcuts.

Algorithm 1 provides a compact procedural specification of the event-aware forecasting pipeline shown in Fig. 4, formalizing the execution order and data dependencies without restating architectural details.

RBA-LSTM Event Prediction Full Pipeline

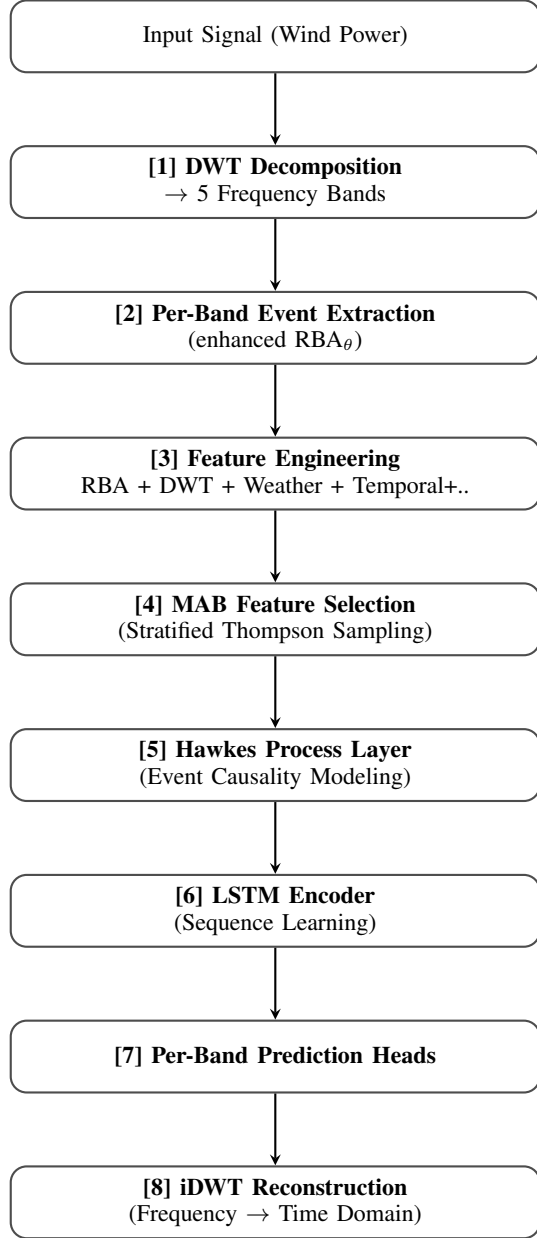


Fig. 4: Full pipeline of Approach 3

D. Approach 4: RBA_θ with Transformer-Based Direct Event Prediction

Approach 4 extends the event-first forecasting paradigm established in Approach 3 by replacing the recurrent sequence encoder with a Transformer. All upstream components like enhanced RBA_θ event extraction, DWT-based multi-resolution processing, Hawkes-based temporal causality, stratified MAB feature selection, band-aware prediction heads, and event-guided reconstruction are *identical* to Approach 3. This strict inheritance ensures that any performance differences can be attributed solely to the temporal modelling backbone. The central question addressed by Approach 4 is therefore: *given the same event representation, features, horizons and objectives, does a self-attention-based encoder provide complementary advantages over recurrence for modelling wind-power event dynamics?*

1) *Transformer Encoder with Horizon-Specific Pathways*: Instead of an LSTM, Approach 4 employs a Transformer encoder to model temporal dependencies across the event-aware feature sequence. Given an input window $\tilde{X}_{1:S} \in \mathbb{R}^{S \times F}$, the encoder computes

$$\begin{aligned} Z^{(0)} &= \text{PE}(\tilde{X}), \\ Z^{(\ell)} &= \text{EncoderBlock}\left(Z^{(\ell-1)}\right), \quad \ell = 1, \dots, L_{\text{enc}}. \end{aligned} \quad (24)$$

where $\text{PE}(\cdot)$ denotes learned positional encoding. The final latent state z_T is obtained via mean pooling over the temporal dimension and is passed to the same frequency-aware prediction heads used in Approach 3.

A key architectural addition is a *dual-pathway design* for short horizons ($H \leq 1$ h). Short-horizon prediction is dominated by local persistence and derivative patterns, whereas longer horizons depend on distributed precursors. To prevent interference between these regimes, Approach 4 includes a lightweight Transformer pathway with reduced depth and dimensionality dedicated to short horizons, while the full encoder is used for longer horizons. This separation stabilises optimisation and improves horizon-specific fidelity.

2) *Loss Function Adaptation*: The multi-task structure and band-aware weighting scheme are inherited from Approach 3. However, the regression losses for magnitude and duration are modified to better align with Transformer training stability. For each band B and horizon H , the loss components are defined as:

$$L_{\text{evt}}(B, H) = \text{BCE}(\hat{y}_{\text{evt}}^{(B)}(t+H), y_{\text{evt}}^{(B)}(t+H)), \quad (25)$$

$$L_{\text{mag}}(B, H) = \frac{1}{N} \sum_t (\hat{y}_{\text{mag}}^{(B)}(t+H) - y_{\text{mag}}^{(B)}(t+H))^2, \quad (26)$$

$$L_{\text{dur}}(B, H) = \frac{1}{N} \sum_t |\hat{y}_{\text{dur}}^{(B)}(t+H) - y_{\text{dur}}^{(B)}(t+H)|. \quad (27)$$

Mean squared error (MSE) is used for magnitude regression to preserve sensitivity to amplitude deviations, while mean

Algorithm 2 Approach 4: Event-Aware Transformer Forecasting

Require: Wind-power series $P(t)$, prediction horizons \mathcal{H}
Ensure: Event predictions (occurrence, type, timing, magnitude, duration and optional reconstructed trajectory)

- 1: Extract enhanced RBA $_\theta$ events and DWT bands
- 2: Construct Hawkes-based temporal features and statistical descriptors
- 3: Select 75 features using horizon-aware stratified MAB
- 4: **for** each horizon $H \in \mathcal{H}$ **do**
- 5: Encode input sequence using Transformer encoder
- 6: Predict event occurrence, type, timing
- 7: Predict band-wise magnitude and duration
- 8: **end for**
- 9: Optionally reconstruct trajectory via inverse DWT

absolute error (MAE) is used for duration to reduce bias toward over-smoothing. The total loss per horizon is

$$L_{\text{total}}(H) = \sum_B \left(\lambda_1 L_{\text{evt}}(B, H) + \lambda_2 L_{\text{mag}}(B, H) + \lambda_3 L_{\text{dur}}(B, H) \right). \quad (28)$$

with the same task and band weights as in Approach 3. Approach 4 follows the same workflow as Approach 3 only the sequence encoder differs.

TABLE III: Key Hyperparameters for Approach 4

Parameter	Value
Transformer layers	2
Attention heads	8
Hidden dimension	128
Dropout rate	0.45
Sequence length	48 hours
Feature dimension	75 (MAB-selected)
Prediction horizons	{1, 6, 12, 24} h
Loss (mag / dur)	MSE / MAE
Optimiser	AdamW

The shallow Transformer depth limits overfitting under limited data, while high dropout counteracts attention overconfidence as shown in table III. Sequence length and feature dimension mirror Approach 3 to preserve comparability.

III. AGENTIC WORKFLOW ORCHESTRATION FOR WIND POWER EVENT PREDICTION

The four workflows developed in Approaches 1-4 are intentionally complementary. Each exhibits different strengths depending on dataset dynamics, horizon length, and event regime. This motivates a final step beyond model design: a self-learning orchestration layer that selects the most suitable workflow for a given dataset and operational context.

Workflow selection was formulated as a *contextual multi-armed bandit* (CMAB) problem, where each workflow is an arm and the dataset itself provides the context. Let

$$\mathcal{W} = \{w_1, w_2, w_3, w_4\}$$

denote the candidate workflows, corresponding to Approach 1-4 respectively. For any dataset D , compact statistical and dynamical fingerprints were extracted capturing volatility, stationarity, trend strength, regime dynamics, entropy, multi-lag autocorrelation and predictability indicators. This context

enables knowledge transfer across heterogeneous wind farms without site-specific hand-tuning.

A. Dataset Similarity and Experience Retrieval

To reuse prior executions, similarity between two datasets D_1 and D_2 using cosine similarity in the context space were quantified:

$$\text{sim}(D_1, D_2) = \frac{\mathbf{C}(D_1)^\top \mathbf{C}(D_2)}{\|\mathbf{C}(D_1)\|_2 \|\mathbf{C}(D_2)\|_2}. \quad (29)$$

Given a similarity threshold $\tau \in (0, 1)$, a neighbourhood of past executions from a persistent experience base \mathcal{E} were retrieved:

$$\mathcal{E}_{\text{sim}} = \{E_j \in \mathcal{E} : \text{sim}(D_j, D) > \tau\}. \quad (30)$$

Each record E_j stores the dataset context, the selected workflow, evaluation metrics, timestamp and a scalar reward R_j (defined below). This provides a lightweight mechanism for context-conditioned decision making.

B. Contextual Reward and Utility

A composite reward that jointly reflects forecasting fidelity, event-level detection quality and computational efficiency was defined. For an execution of workflow w_i on dataset D , the reward is

$$R(w_i, D) = 0.4 R_{\text{test}}^2 + 0.2 \left(1 - \frac{\text{MAE}_{\text{test}}}{500} \right) + 0.3 F_{\text{events}} + 0.1 \left(1 - \frac{t_{\text{exec}}}{3600} \right). \quad (31)$$

where R_{test}^2 and MAE_{test} measure predictive accuracy, F_{events} measures event detection quality, and t_{exec} is total execution time in seconds. The constants normalise each component to comparable scale and emphasise event-relevant performance.

C. Weighted Value Estimation from Similar Executions

For each workflow w_i , a context-conditioned expected utility by a weighted average over similar executions was estimated:

$$Q(w_i, \mathbf{C}) = \frac{\sum_{E_j \in \mathcal{E}_{\text{sim}}(w_i)} \gamma_j R_j}{\sum_{E_j \in \mathcal{E}_{\text{sim}}(w_i)} \gamma_j}, \quad (32)$$

where $\mathcal{E}_{\text{sim}}(w_i)$ denotes similar executions using workflow w_i , and γ_j is a reliability weight that down-weights stale, synthetic or low-confidence evidence. γ_j is a product of three interpretable factors:

$$\gamma_j = \gamma_j^{(\text{rec})} \gamma_j^{(\text{src})} \gamma_j^{(\text{conf})}. \quad (33)$$

The recency term applies exponential decay so that recent evidence dominates:

$$\gamma_j^{(\text{rec})} = \exp\left(-\frac{\Delta t_j}{30}\right), \quad (34)$$

TABLE IV: Comparison of the four approaches for wind-event prediction

Aspect	Approach 1	Approach 2	Approach 3	Approach 4
Core idea	Classical forecasting with post hoc event detection.	Static event features with RF classification and survival-based timing.	Deep multi-band sequence modelling with Hawkes-based temporal causality.	Same as Approach 3, replacing LSTM with Transformer.
Frequency handling	None.	Limited hand-crafted features.	DWT-based multi-resolution processing.	Same as Approach 3.
Causality modelling	None.	Implicit (static RF).	Hawkes intensities for temporal clustering.	Self-attention and Hawkes causality.
Feature selection	Manual.	Manual filtering.	Stratified multi-armed bandit.	Stratified multi-armed bandit.
Reconstruction	None.	None.	Event-guided reconstruction via DWT.	Same as Approach 3.
Event prediction	Post hoc, threshold-based.	Event-first with limited generalisation.	Event-first with strong generalisation.	Same as Approach 3.
Horizon support	Not implemented.	Not implemented.	Multi-horizon (1, 6, 12, 24 h).	Multi-horizon (1, 6, 12, 24 h).
Magnitude / duration	Not explicitly modelled.	Not modelled.	Per-band magnitude and duration prediction.	Same as Approach 3.
Zero-shot transfer	Not supported.	Not supported.	Moderate-to-good generalisation.	Moderate-to-good generalisation.
Scalability	Low; per-site tuning required.	Moderate; tree models remain site-specific.	High.	High.
Operational fit	High interpretability, low accuracy.	Moderate interpretability and accuracy.	High event fidelity with physical structure.	Highly competitive operational relevance.

where Δt_j is the age of execution E_j measured in days. The source term ensures that synthetic bootstrap knowledge decays as real data accumulates:

$$\gamma_j^{(\text{src})} = \alpha^{n_{\text{real}}}, \quad \alpha = 0.95, \quad (35)$$

where n_{real} is the number of real executions stored so far. Finally, the confidence term penalises workflows with limited evidence in the retrieved neighbourhood:

$$\gamma_j^{(\text{conf})} = \min\left(\frac{n_i}{5}, 1\right), \quad (36)$$

where n_i is the number of similar executions available for workflow w_i . Together, (33)–(36) yield a practical estimator that is robust to stale logs, cold-start priors and sparse coverage.

D. Exploration-Exploitation with UCB and Adaptive ϵ

Given $Q(w_i, \mathbf{C})$, the ideal choice is

$$w^* = \arg \max_{w_i \in \mathcal{W}} \mathbb{E}[R(w_i, D) | \mathbf{C}(D)], \quad (37)$$

which was approximated by maximising $Q(w_i, \mathbf{C}(D))$ when exploiting. To avoid over-commitment under uncertainty, the agent also explores using an upper-confidence strategy:

$$\text{UCB}(w_i, \mathbf{C}) = Q(w_i, \mathbf{C}) + c\sqrt{\frac{\ln N}{n_i}}, \quad c = 2.0, \quad (38)$$

where $N = \sum_i n_i$ is the total number of similar executions and n_i is the count for workflow w_i . This encourages exploration when n_i is small. Exploration is controlled using an adaptive ϵ -greedy policy:

$$\epsilon(t) = \epsilon_{\text{base}} f_{\text{contr}} f_{\text{local}} f_{\text{cons}} f_{\text{data}}, \quad \epsilon_{\text{base}} = 0.2, \quad (39)$$

with $\epsilon(t) \in [0.05, 0.60]$. The multiplicative factors increase exploration when contradictions are detected between synthetic and real evidence, when selection concentrates on a single workflow, or when the agent has repeatedly exploited without testing alternatives. This improves robustness under dataset shift and prevents premature convergence.

E. Contradiction Detection and Bootstrap Decay

To prevent bootstrap bias, contradictions between synthetic bootstrap executions and real executions are explicitly detected. Let \mathcal{S} and \mathcal{R} denote the subsets of retrieved similar executions originating from synthetic priors and real runs, respectively; then the source-specific best workflow is defined as:

$$w_{\mathcal{S}}^* = \arg \max_{w_i \in \mathcal{W}} \mu_{\mathcal{S}}(w_i), \quad w_{\mathcal{R}}^* = \arg \max_{w_i \in \mathcal{W}} \mu_{\mathcal{R}}(w_i), \quad (40)$$

where $\mu_{\mathcal{S}}(w_i)$ and $\mu_{\mathcal{R}}(w_i)$ denote mean rewards under each source. A contradiction is flagged when

$$w_{\mathcal{S}}^* \neq w_{\mathcal{R}}^*, \quad |\mu_{\mathcal{S}}(w_{\mathcal{S}}^*) - \mu_{\mathcal{R}}(w_{\mathcal{R}}^*)| > 0.10, \quad |\mathcal{R}| \geq 3.$$

When this occurs, Synthetic evidence is discarded for the current decision and increase exploration, ensuring that real evidence dominates selection as soon as it is sufficiently informative.

F. Learning Loop and Persistent Memory

After selecting a workflow and executing it, the agent computes $R(w^*, D)$ using (31) and appends a new record to the experience base \mathcal{E} . This yields a self-improving loop: each run refines future estimates via (32), while the bootstrap influence decays automatically through (35). In effect, the system does not only learn event predictors; it learns *which* predictor to

trust under which dataset conditions. This closes the methodological loop of the paper by integrating Approaches 1–4 into a unified, adaptive decision-making layer that targets robust wind-power event prediction under heterogeneous operating regimes.

IV. RESULTS AND ANALYSIS

A. Dataset Description and Environmental Setup

The proposed event-centric and frequency-aware forecasting framework is evaluated using multiple offshore wind datasets that differ in geographical location, meteorological regimes, and operational characteristics. The usage of the datasets are summarized in Table V. This design supports both in-distribution evaluation and strict zero-shot generalisation to unseen wind farms.

The primary training and validation dataset corresponds to the Baltic Eagle offshore wind farm and is obtained from the publicly available “40 Years of European Offshore Wind” dataset generated using the Copernicus Climate Change Service (C3S) ERA5 reanalysis [25]. The dataset provides 40 years (1980–2019) of hourly observations including hub-height wind information, wind direction, surface roughness, and turbine- and farm-level power output. Model development, feature selection, and hyperparameter tuning are performed exclusively on Baltic Eagle using a chronological split: 70% training, 15% validation, and 15% test, ensuring no temporal leakage. To evaluate zero-shot transferability, two additional offshore wind farms from the same repository are used without any retraining or adaptation.

One of them is Baie de Saint-Brieuc (English Channel) data that exhibits strong mesoscale variability influenced by Atlantic inflow and boundary-layer transitions, while the other one i.e., London Array (Thames Estuary) dataset reflects frequent frontal activity and complex turbulence and wake interactions. For both transfer datasets, the evaluation strictly uses only variables provided in the original dataset to preserve the integrity of the zero-shot setting. An additional Estonian coastal capacity-factor dataset with eight-turbines, also used in earlier RBA_θ studies [4], [5], is employed only during initial baseline development and algorithm validation and is excluded from all final learning-based evaluations due to its synthetic nature and limited temporal depth.

Power output is normalised by dividing by the nominal (rated) capacity to obtain a unit-scale series consistent across sites. All experiments are conducted on a standard desktop system equipped with a quad-core Intel CPU operating at 2.0 GHz and 16 GB of RAM. The implementation is written in Python 3.9. The complete implementation is available at this Github link.

B. Analysis and Discussions

This section evaluates the proposed event-aware, frequency-informed forecasting framework introduced in Section II. The analysis mostly focuses on the two competitive deep workflows (Approach 3 and Approach 4), while classical baselines are used to contextualise performance gains.

TABLE V: Summary of dataset roles across the workflow

Dataset	Model Training	Event Extraction	Zero-Shot Transfer
Baltic Eagle	Yes	Yes	–
Baie de Saint-Brieuc	–	Yes	Yes
London Array	–	Yes	Yes
Eight-Turbine Dataset	Initial development	Baseline only	–

To expose the temporal structure of wind-power variability across scales, the power time series is decomposed using Discrete Wavelet Transform (DWT) into one approximation component and four detail components, as illustrated in Fig. 5. The original series exhibits a mean of 224.81 MW, a standard deviation of 168.82 MW, and a range spanning [0, 475] MW, indicating substantial variability driven by atmospheric dynamics.

The approximation band captures slow-varying background behaviour, with statistics (mean 224.76 MW, std 157.55 MW) closely matching the original signal. Its wide amplitude range reflects long-term regime shifts and seasonal structure, but it carries limited information about rapid ramp events. In contrast, the detail bands isolate progressively faster dynamics. Among them, the D_3 band (approximately 2–8 h) exhibits the largest variance (std 16.81 MW) and the widest range among the mid-frequency components, indicating that it concentrates most ramp-related energy. The D_4 band (8–16 h) contributes smoother sub-diurnal fluctuations, while the higher-frequency bands (D_2, D_1) show increasing variance dominated by short-term oscillations and noise rather than coherent ramp structure. These statistics justify focusing predictive attention on mid-frequency bands for event characterisation, while treating the highest-frequency components primarily as noise carriers and the approximation band as a reconstruction scaffold.

Across all experimental workflows, adaptive feature selection consistently highlights a common set of physically meaningful predictors. Event-derived quantities (such as event magnitude, duration, density and timing) form the most stable contributors to event occurrence and classification. Wavelet-based features from the mid-frequency bands, particularly variance, energy and cross-band ratios, repeatedly emerge as strong indicators of ramp intensity and persistence. Meteorological drivers related to pressure gradients, wind-speed evolution and synoptic forcing provide complementary context, while temporal encodings (hour-of-day, cyclic seasonality) support alignment with diurnal and seasonal patterns. Nonlinear interaction terms further capture compound effects that are not apparent from marginal statistics alone. These observations indicate that reliable wind-event prediction relies on a balanced combination of event semantics, mid-scale frequency structure and physically grounded atmospheric cues. Adaptive selection mechanisms, such as bandit-based exploration, consistently converge towards this combination, reinforcing that the identified features reflect genuine wind-power physics rather than artefacts of a particular model or dataset.

Based on this foundation, forecasting results are mostly reported along six axes: event prediction accuracy, event

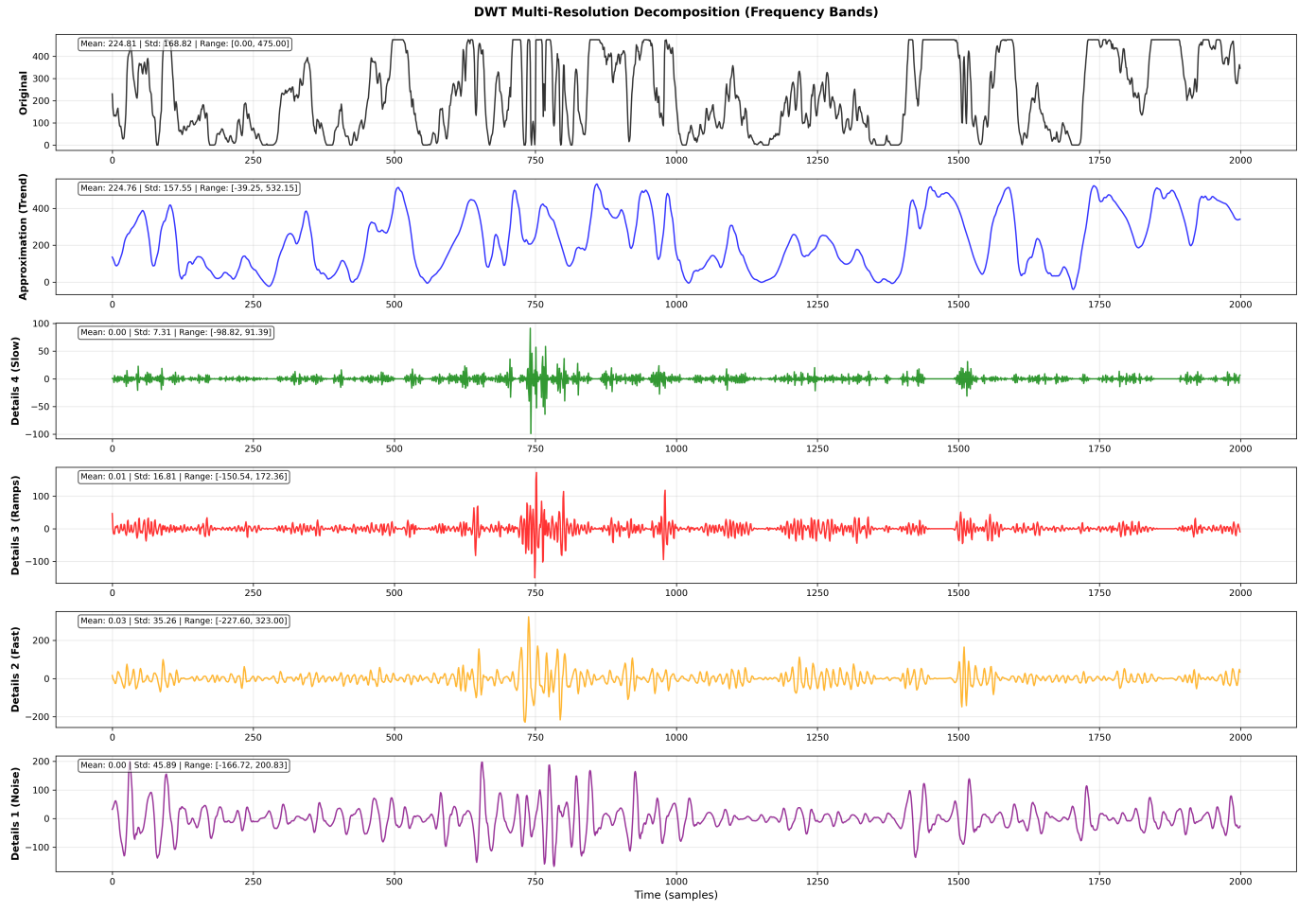


Fig. 5: DWT decomposition of the wind-power time series into approximation and detail bands.

magnitude and duration estimation, signal reconstruction fidelity, computational costs, ablation studies, and zero-shot transferability across wind farms.

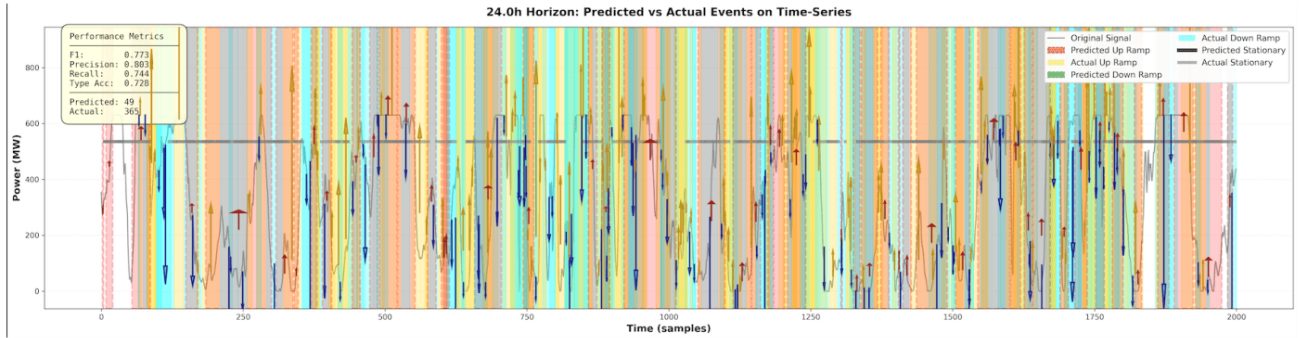
1) *Event Prediction*: Event prediction quality is assessed mostly using precision, recall, and F1-score across forecasting horizons from 1 h to 24 h. Precision is emphasised due to its operational importance in ramp-alert systems.

Approach 1 provides a strong interpretable reference, achieving F1 of 0.91 on the Baltic Eagle dataset with low false-alarm rates. This establishes an upper-bound for rule-based post-hoc extraction and motivates direct event prediction. Approach 2 formulates event prediction as a direct classification problem using a two-stage RF-RBA_θ pipeline. The survival-analysis variant exhibits a clear performance ceiling with the best Kaplan-Meier fallback model configuration attaining a F1 score of 0.41 with precision of ≈ 0.38 and the recall was ≈ 0.46. Weibull-AFT completely failed to run, mainly due to mathematical instability (failed matrix inversion), high collinearity among covariates, and severe event sparsity.

Replacing survival modelling with a pointwise Random Forest classifier substantially improves predictive capacity. On the Baltic Eagle test split, the RF baseline achieves a precision of 0.76 with 83.5% relative improvement in F1-score over the

survival baseline. This establishes Approach 2 as the strongest non-deep reference model for direct event occurrence and type prediction. A class-wise analysis further reveals asymmetric behaviour. For significant ramps, the classifier is conservative, achieving precision ≈ 0.85 and recall ≈ 0.62, while for stationary periods it prioritises coverage, with recall ≈ 0.93 and precision ≈ 0.70. This precision–recall trade-off aligns with operational priorities and provides a meaningful quantitative baseline against which the deep event-predictive workflows (Approaches 3 and 4) are evaluated. For Approach 3, event prediction performance improves monotonically with horizon. At short horizons (1 h), recall is high but precision is limited due to noise sensitivity. At longer horizons (12–24 h), the model achieves balanced performance with relatively high precision of ≈ 0.84 in context of direct event prediction, indicating reliable early identification of coherent ramp structures. Approach 4 exhibits a more conservative prediction profile. While short-horizon performance is weaker, precision improves steadily with horizon and peaks at ≈ 0.78 at 24 h. Compared to the LSTM, as shown in Fig 6, the Transformer produces smoother and less fragmented event sequences, at the cost of missing some shorter ramps. This qualitative comparison confirms the quantitative trends: short-horizon predictions are reactive, while longer horizons yield stable and

Predicted vs actual events for approach 3



Predicted vs actual events for approach 4

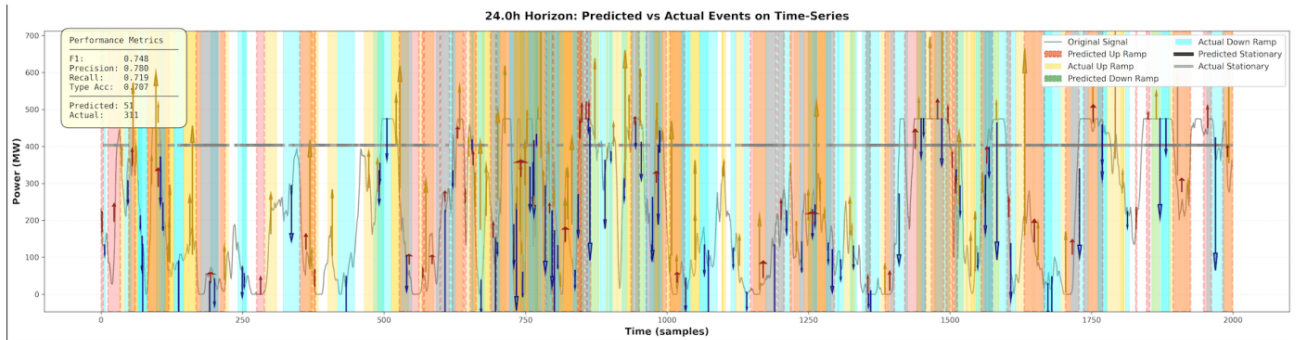


Fig. 6: Comparison of predicted and true events for 24-hour horizon using Approach 3 & 4

operationally useful segmentation.

2) *Magnitude and Duration Prediction*: Event severity is quantified through magnitude and duration regression. Performance is evaluated using the coefficient of determination (R^2) computed separately for each DWT frequency band as shown in Figure 7.

In case of Approach 3, Magnitude prediction exhibits strong frequency selectivity. The mid-frequency ramp band (Details_3) dominates performance, as it contains the most ramp energies, reaching R^2 of 0.33 at 24 h. High-frequency bands remain non-predictive, indicating effective noise suppression. Duration prediction is more challenging but improves with horizon, with Details_4 reaching $R^2 \approx 0.46$ at 24 h. On the other hand, approach 4 preserves the same frequency structure but with smoother behaviour. Magnitude prediction in Details_3 reaches $R^2 \approx 0.27$ at long horizons, slightly below the LSTM peak but more stable across horizons. Duration prediction remains weaker overall, suggesting that recurrent inductive bias better captures persistence. These results demonstrate that

(i) ramp magnitude is governed primarily by mid-frequency dynamics,

(ii) duration requires fine-scale temporal continuity, and

(iii) both models correctly suppress low-information bands.

3) *Signal Reconstruction Performance*: Reconstruction evaluates whether predicted events encode sufficient informa-

tion to recover physically meaningful power trajectories. It has been performed using the method discussed in Subsection II-C3.

Approach 3 achieves the best reconstruction fidelity, with $\text{RMSE} \approx 51.1 \text{ MW}$ and R^2 of 0.90 on Baltic Eagle. Approach 4 follows closely with $R^2 \approx 0.84$, producing smoother but slightly attenuated ramps. A comparative reconstruction of both approaches is shown in Figure 8. The other methods shown in figure were also applied for comparative analysis where "Simple Event" i.e, our approach turns out to be the best reconstruction method. The other two methods failed because it only uses the poor prediction of Approximation band as base which causes high mismatch. "Simple Event" instead match trends between recent past and prediction and smartly decides the nature of the baseline that actually align closely with the actual Approximation band. These results confirm that event-aware reconstruction is feasible only when combined with frequency-aware signal anchoring. Pure event-only reconstruction fails to preserve global trends, while deterministic approximation stabilises long-range structure. It also shows, event aware predictions and then reconstruction can be highly competitive to the traditional time-series forecasting. As the data is shrunk into events, computational cost for complex high volume dataset also gets reduced as discussed in the next point.

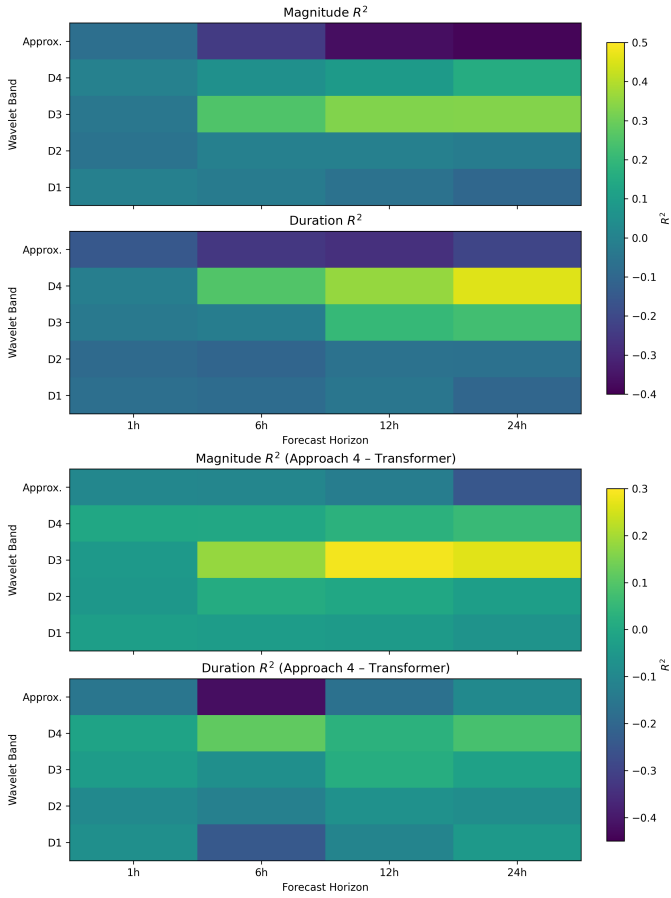


Fig. 7: Per-band R^2 heatmaps for magnitude (top) and duration (bottom). Approach 3 shown above, and Approach 4 below

4) *Computational Cost Analysis*: Operational feasibility of event-aware forecasting depends critically on training and inference cost. This subsection evaluates the computational overhead of all four approaches and clarifies the trade-off between runtime and semantic richness.

a) *Training cost*: Table VI reports training and total execution times. Classical approaches are computationally efficient: SARIMAX-RBA $_{\theta}$ completes training in ≈ 6 minutes, while the Random Forest baseline requires ≈ 50 minutes due to its expanded feature space. Representing the complex time-series in terms of significant and stationary events also helped to compress the data, amplifying the model learning times. This was further proven when SARIMAX was integrated with RandomForest classifier instead of RBA $_{\theta}$ removing the influence of event-level features. SARIMAX-RF took 3 more minutes to train, which shows incorporating event semantics brings the possibility to improve computational cost associated to complex analytical and forecasting tasks. Although, the deep event-aware workflows incur substantially higher computational cost compared to first two approaches, with Approach 3 (LSTM) and Approach 4 (Transformer) requiring over 300 and 400 minutes, respectively. This overhead mainly arises from the inherent complex architecture.

b) *Inference cost for zero-shot deployment*: Inference time follows a similar trend. Table VII detail zero-shot transfer

TABLE VI: Training and total computation times for all forecasting approaches

Approach	Training Time	Total Runtime
Approach 1	6.04 min	≈ 8 min
Approach 2	50.40 min	55.80 min
Approach 3	315.70 min	334.13 min
Approach 4	399.17 min	418.33 min

TABLE VII: Zero-shot inference time for Approach 3 and Approach 4.

Approach 3	
Component	Time (s)
event_extraction	175.97
model_prediction	315.55
Total	579.48

Approach 4	
Component	Time (s)
event_extraction	179.92
model_prediction	485.48
Total	750.46

runtimes. The dominant contributors are RBA $_{\theta}$ event extraction and deep model inference, particularly for the Transformer due to global attention. Even so, total inference time remains below 13 minutes per unseen wind farm, which is acceptable for hourly or day-ahead operational use.

While deep workflows are computationally heavier, they produce substantially richer outputs such as event occurrence, magnitude, duration, frequency structure, and physically coherent reconstructions. This semantic gain justifies the additional cost and supports deployment in scenarios where decision quality outweighs raw speed.

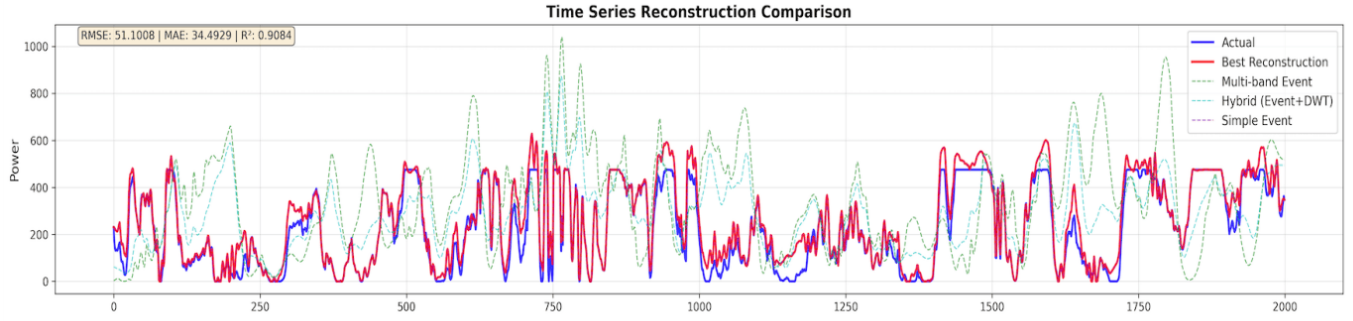
C. Ablation Studies

This section isolates the contribution of event semantics and adaptive feature selection within the proposed framework. Two complementary ablation levels are considered. First, a classical baseline ablation evaluates whether explicit RBA $_{\theta}$ event semantics provide information beyond pointwise statistical classifiers when applied to SARIMAX forecasts. Second, component ablations are conducted on the deep event-prediction backbone (Approach 3) to quantify the individual impact of RBA $_{\theta}$ -derived features and multi-armed bandit (MAB) feature selection. Since signal reconstruction relies on the DWT approximation band, no DWT-removal ablation is performed.

1) *Baseline Ablation: SARIMAX with and without RBA $_{\theta}$ Information*: Two variants are compared that are a post-hoc RBA $_{\theta}$ event extraction pipeline (Approach 1) and a similar SARIMAX integrated to a RandomForest Classifier for event classification removing the influence of RBA $_{\theta}$ event semantics. While both approaches yield comparable trajectory accuracy, their event-prediction capability differ markedly.

In power forecasting, Approach 1 achieves a lower mean absolute error (15.36 kW versus 16.57 kW), whereas

Reconstruction – approach 3



Reconstruction – approach 4

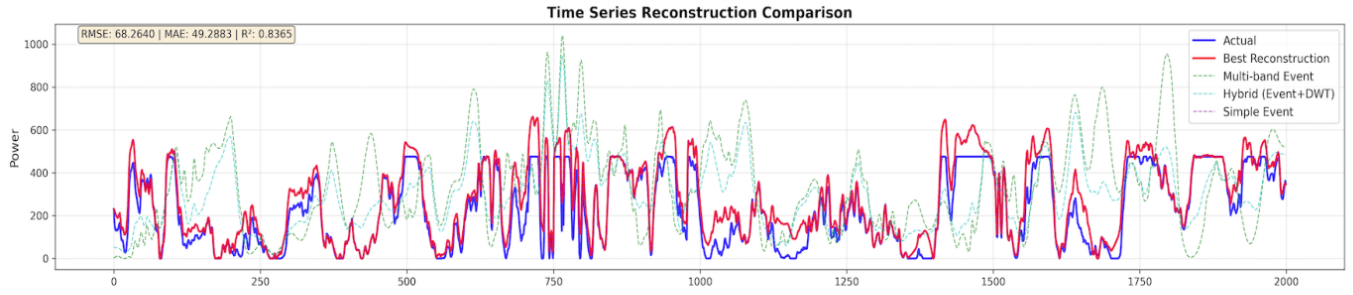


Fig. 8: Final reconstructed trajectory from predicted events using approach 3 and approach 4

SARIMAX–RF attains a lower RMSE (18.04 kW versus 23.03 kW) and a slightly higher coefficient of determination ($R^2 = 0.9896$ versus 0.9830). Despite similar trajectory fidelity, event prediction performance diverges strongly. Post-hoc RBA_θ extraction achieves an F1-score of 0.91, corresponding to a relative improvement of +16.8% compared to SARIMAX–RF. Precision and recall increase by approximately +14.2% and +19.5%, respectively. This gap demonstrates that the temporal ramp grammar encoded by RBA_θ cannot be recovered reliably from pointwise statistical features alone. The SARIMAX–RF pipeline remains competitive primarily for stationary regimes ($F1 \approx 0.93$), where temporal structure is weak and event boundaries are less informative.

2) *Deep-Model Ablations: Event Semantics and Feature Selection:* Component ablations are next conducted on the deep event-prediction backbone to quantify the role of semantic inputs and adaptive feature selection. We started with a vanilla LSTM baseline that uses ground-truth event labels for supervision but does not ingest RBA_θ -derived features. An event-aware variant augments the same backbone with RBA_θ inputs. Additional ablations remove RBA_θ features or disable MAB selection within Approach 3. Table VIII summarises the quantitative impact of these ablations, focusing on precision and F1 as operationally relevant metrics. For Approach 3 component ablations, results are reported at 1 h and 24 h horizons to contrast short-horizon noise sensitivity against

TABLE VIII: Ablation summary for approach 3 in terms of precision and F1

Setting	Precision	F1
Vanilla LSTM (no RBA inputs)	0.9764	0.9787
RBA_θ -augmented LSTM	0.9751	0.9793
Approach 3 without MAB (1 h)	≈ 0.26	0.39
Approach 3 without RBA_θ features (1 h)	≈ 0.06	0.09
Approach 3 without RBA_θ features (24 h)	≈ 0.64	0.64
Approach 3 without MAB (24 h)	≈ 0.81	0.75

long-horizon temporal context.

Augmenting a strong LSTM backbone with RBA_θ features yields only a marginal absolute gain in F1 (+0.06%), reflecting that the vanilla model already fits the labels well. However, this comparison is performed under a deliberately coarse binary formulation, where the task is limited to predicting whether an event occurs or not, without resolving event type, magnitude, or temporal structure. Under this setting, predictions are inherently noisy and information-poor, which constrains the observable benefit of semantic augmentation. The consistent improvement nonetheless indicates that RBA_θ features act as a semantic regulariser rather than a capacity expansion mechanism, with their primary advantage emerging in structured, multi-class and horizon-aware event settings rather than in binary detection alone.

In contrast, removing RBA_θ features from the Approach 3 backbone causes a severe performance collapse at short horizons, with F1 dropping to 0.09 at 1 h. Even with increased temporal context at 24 h, performance recovers only partially (F1 and precision ≈ 0.64), demonstrating that explicit event semantics are essential for stabilising ramp discrimination under short-term turbulence.

Disabling MAB feature selection also degrades performance, though less catastrophically than removing semantic inputs. At 1 h, F1 drops to 0.39, consistent with high-dimensional feature noise overwhelming the learner. At 24 h, performance recovers F1 to 0.75, but remains inferior to the full model, indicating residual sensitivity to feature redundancy. While mutual-information-based selection avoids complete collapse, it does not match the robustness of adaptive, horizon-aware MAB selection. Overall, the ablation results establish a clear hierarchy of contributions. RBA_θ features provide the dominant gain in robustness at short horizons, where false alarms and boundary fragmentation are most likely. MAB feature selection is critical for preventing feature overload and preserving precision-oriented behaviour as the candidate feature pool exceeds approximately 1,400 dimensions. Reliable event-aware forecasting therefore requires both explicit semantic inputs and adaptive feature selection to remain stable under operational noise and regime variability.

D. Zero-Shot Transfer Across Wind Farms

Generalisation is evaluated by applying Baltic Eagle-trained models to Baie de Saint-Brieuc and London Array without retraining. Approach 4 achieves:

$$F1_{24h} \approx 0.62, \quad \text{Precision}_{24h} \approx 0.60$$

on Baie de Saint-Brieuc, with successful trajectory reconstruction from the predictions. Similar performance is achieved for the other dataset as well which proves the consistency in performance.

Approach 3 yields comparable reconstruction accuracy with 5% higher precision but with the same (5%) lower F1-score. Both approaches repetitively produced around 0.60 precision in event prediction on completely unseen data, that too completely without fine-tuning. These results demonstrate that DWT representations and RBA_θ event semantics encode somewhat site-invariant structure that transfers across geophysical regimes. Across all experiments, three consistent findings emerge. First, event predictability increases with horizon as temporal context aligns with physical ramp formation scales. Second, magnitude and duration information concentrates in mid-frequency bands, validating the frequency-aware design. Third, reconstruction fidelity and transferability confirm that event-first representations provide a robust abstraction for operational wind-power forecasting. Together, these results establish the proposed framework as a practical and generalisable alternative to trajectory-first forecasting, offering improved semantic clarity, robustness, and cross-site applicability.

E. Agentic Workflow Selection

The agentic system was validated on Baltic Eagle wind farm data (350,640 samples, 40-year ERA5 reanalysis). Bootstrap

initialization from 8 expert rules provided 72 synthetic priors. On the first real execution, the agent detected local optimum (Approach/Workflow 3 over-represented at 38.9%) and forced exploration of Workflow 1(SARIMAX-RBA). Despite forced intervention, Workflow 1 achieved R^2 of 0.98, MAE of 15.57, and F1 of 0.91, establishing a reward of 0.820. With adaptive exploration and contradiction detection, the system achieves more and more accurate workflow selection capability after multiple executions, with cumulative reward improvement over fixed rules. Stratified sampling enables sub-3-second data characterization even for large datasets while maintaining minimal feature extraction error, making the system suitable for real-time deployment.

V. LIMITATIONS

Despite the strong empirical performance of the proposed event-aware forecasting framework, several limitations remain. First, unlike LSTM-based Approach 3, horizon-specific Transformer models required several hours of training, and removing core components such as RBA_θ inputs or MAB feature selection for ablation frequently destabilised attention and led to non-convergent training. As a result, the contribution of individual components in Approach 4 could not be isolated. Second, short-horizon event prediction (1-3 h) still remains challenging. Although adaptive feature selection and frequency-domain representations improve performance over classical baselines, precision and R^2 are substantially lower than at longer horizons. This limitation might be due to the absence of numerical weather prediction inputs, as short-term wind ramps are often driven by mesoscale phenomena not inferable from historical data alone.

Third, generalisation across heterogeneous domains has not yet been established. Zero-shot application to a different dataset was not feasible mostly due to fundamental feature mismatch and domain-specific data constraints. Remodification of the workflows in context of those datasets were also performed and currently the multivariate prediction part is highly dependent on input data quality and balance across variables. When individual entities (e.g., price zones or turbines) exhibit strong imbalance, sparsity, or inconsistent dynamics, model performance degrades substantially. In contrast, when data quality is high and sufficiently long temporal context is available for training, the model exhibits strong performance. The current design therefore favours data-rich settings and is not yet suitable for short or highly imbalanced datasets, limiting its applicability across heterogeneous domains.

Fourth, explicit uncertainty quantification could not be incorporated due to computational constraints. Bayesian techniques such as Monte Carlo dropout, deep ensembles, and probabilistic inference were incompatible with the memory and training requirements of the multi-band LSTM and Transformer models. While RBA_θ and Hawkes Causality implicitly captures event-level uncertainties through persistence and boundary variability, calibrated probabilistic estimates are not provided.

Lastly, the event extraction stage relies on enhanced RBA_θ -Traditional thresholding method which is statistical based.

Bayesian adaptive thresholding via RBA_{θ} RF-MCMC was omitted due to its high computational cost. The evaluation is constrained by dataset and modelling scope. Experiments primarily rely on reanalysis or synthetic data and do not capture operational SCADA effects such as curtailment or sensor faults. Moreover, the framework models a single wind farm at a time and does not account for spatial interactions, limiting applicability in multi-farm settings. These limitations arise from computational constraints, data availability, and the intrinsic complexity of atmospheric dynamics, and they define clear directions for future work.

VI. CONCLUSION AND FUTURE SCOPE

This work advances wind-power forecasting by reframing it as an *event-centric, frequency-aware, and agentically coordinated* problem rather than a dense trajectory regression task. Motivated by the operational reality that power-system decisions depend on the timing, magnitude, duration, and persistence of events, the proposed framework aligns forecasting objectives with decision-making needs. Empirical results across multiple workflows demonstrate that wind-power ramps are inherently multi-scale phenomena, with predictive information concentrated in specific mid-frequency bands. Embedding enhanced RBA_{θ} event semantics, multi-resolution signal decomposition, and adaptive feature selection directly into the learning pipeline enables stable event prediction and physically coherent reconstruction. Reconstruction achieves competitive trajectory accuracy ($R^2 \approx 0.90$) while ablation studies confirm that event semantics and adaptive feature selection are structural requirements rather than auxiliary enhancements. Comparative analysis further shows that LSTM- and Transformer-based workflows offer complementary strengths, motivating an agentic forecasting paradigm in which specialised models are dynamically selected based on horizon, uncertainty, and data characteristics rather than enforcing a single monolithic solution.

Future work extends naturally from these findings along three primary directions. First, incorporating spatial and graph-based models can enable explicit modelling of spatial correlations and event propagation across turbines, wind farms, or market zones, capturing inter-location autocorrelation effects that are not addressed in the current single-site formulation. Second, formalising multivariate event prediction remains an important extension, including principled treatment of variable coupling, data imbalance across entities, and context requirements for reliable learning in high-dimensional settings. Third, advancing real-time adaptability under uncertainty is essential for operational deployment. This includes developing lightweight uncertainty-aware mechanisms and adaptive control strategies that allow event-first models to remain stable under streaming data, regime shifts, and rapidly evolving system conditions. Together, these directions aim to generalise the proposed framework beyond wind power and enable scalable, interpretable, and robust forecasting systems for complex energy applications.

REFERENCES

- [1] Sawant, M.; Patil, R.; Shikhare, T.; Nagle, S.; Chavan, S.; Negi, S.; Bokde, N.D. A Selective Review on Recent Advancements in Long, Short and Ultra-Short-Term Wind Power Prediction. *Energies* 2022, 15, 8107. <https://doi.org/10.3390/en15218107>
- [2] Cristobal Gallego-Castillo, Alvaro Cuerva-Tejero, Oscar Lopez-Garcia, A review on the recent history of wind power ramp forecasting, *Renewable and Sustainable Energy Reviews*, Volume 52, 2015, Pages 1148-1157, ISSN 1364-0321. <https://doi.org/10.1016/j.rser.2015.07.154>
- [3] Orlanski, Isidoro. "A Rational Subdivision of Scales for Atmospheric Processes." *Bulletin of the American Meteorological Society*, vol. 56, no. 5, 1975, pp. 527–30. JSTOR, Accessed 4 Feb. 2026. <http://www.jstor.org/stable/26216020>
- [4] P. Sengupta and S. Mishra, "Enhanced RBA_{θ} method for uncertainty quantification in time varying dataset," 2025 12th International Conference on Electrical and Electronics Engineering (ICEEE), Istanbul, Turkiye, 2025, pp. 314-320. 10.1109/ICEEE67194.2025.11261961
- [5] Sambeet Mishra, Esin Ören, Chiara Bordin, Fushuan Wen, Ivo Palu, Features extraction of wind ramp events from a virtual wind park, *Energy Reports*, Volume 6, Supplement 6, 2020, Pages 237-249, ISSN 2352-4847. <https://doi.org/10.1016/j.egyr.2020.08.047>
- [6] Singh , S.K., Jha, S.K. & Gupta, R. A fusion approach of discrete wavelet decomposition and deep learning techniques for the enhancement of wind speed prediction accuracy. *Theor Appl Climatol* 156, 223 (2025). <https://doi.org/10.1007/s00704-025-05450-x>
- [7] Wang, HK., Zhang, X., Long, H. et al. W-FENet: Wavelet-based Fourier-Enhanced Network Model Decomposition for Multivariate Long-Term Time-Series Forecasting. *Neural Process Lett* 56, 43 (2024). <https://doi.org/10.1007/s11063-024-11478-3>
- [8] Robert A. Jacobs, Michael I. Jordan, Steven J. Nowlan, Geoffrey E. Hinton; Adaptive Mixtures of Local Experts. *Neural Comput* 1991; 3 (1): 79–87. <https://doi.org/10.1162/neco.1991.3.1.79>
- [9] Hamilton, James D. "A New Approach to the Economic Analysis of Nonstationary Time Series and the Business Cycle." *Econometrica*, vol. 57, no. 2, 1989, pp. 357–84. JSTOR, Accessed 4 Feb. 2026. <https://doi.org/10.2307/1912559>
- [10] Tilmann Gneiting, Fadoua Balabdaoui, Adrian E. Raftery, Probabilistic Forecasts, Calibration and Sharpness, *Journal of the Royal Statistical Society Series B: Statistical Methodology*, Volume 69, Issue 2, April 2007, Pages 243–268. <https://doi.org/10.1111/j.1467-9868.2007.00587.x>
- [11] Jie Li, Fanxi Meng, Zichen Zhang, Yipu Zhang, Prediction of wind power ramp events via a self-attention based deep learning approach, *Energy Reports*, Volume 12, 2024, Pages 1488-1502, ISSN 2352-4847. <https://doi.org/10.1016/j.egyr.2024.07.023>
- [12] Tingqi Zhang, Junjie Sun, Qiang Zhang, Jifeng Cheng, Peng Yuan, Multi-step prediction of wind power ramping based on dynamic historical window adjustment, *Energy Reports*, Volume 14, 2025, Pages 1708-1716, ISSN 2352-4847. <https://doi.org/10.1016/j.egyr.2025.08.004>
- [13] Yifan Xu. An improved wind power prediction via a novel wind ramp identification algorithm, Version Number: 1. <https://arxiv.org/abs/2502.12807>
- [14] Russell Sharp, Hisham Ihsaish, and J. Ignacio Deza. Integrating wind variability to modelling wind-ramp events using a non-binary ramp function and deep learning models, Version Number: 1. <https://arxiv.org/abs/2211.17017>
- [15] Laura Bianco, Reagan Mendeke, Jakob Lindblom, Irina V. Djalalova, David D. Turner, and James M. Wilczak. Evaluating the ability of the operational high resolution rapid refresh model version 3 (HRRRv3) and version 4 (HRRRv4) to forecast wind ramp events in the US great plains. 10(10):2117–2136. ISSN 2366-7451. 10.5194/wes-10-2117-2025
- [16] Zhang, J.; Zhu, X.; Xie, Y.; Chen, G.; Liu, S. Detection and Prediction of Wind and Solar Photovoltaic Power Ramp Events Based on Data-Driven Methods: A Critical Review. *Energies* 2025, 18, 3290. <https://doi.org/10.3390/en18133290>
- [17] Li, F.; Wang, H.; Wang, D.; Liu, D.; Sun, K. A Review of Wind Power Prediction Methods Based on Multi-Time Scales. *Energies* 2025, 18, 1713. <https://doi.org/10.3390/en18071713>
- [18] Eltohamy, M.S., Abdel Moteleb, M.S., Talaat, H.E.A. et al. A novel approach for power ramps classification in wind generation. *Sci Rep* 13, 21427 (2023). <https://doi.org/10.1038/s41598-023-48443-4>
- [19] Han Y, Wang X, Li K. Wind power prediction with accurate identification of ramp events based on Interval-SMOTE oversampling and ensemble learning. *Wind Engineering*. 2025;49(4):1080-1100. <https://10.1177/0309524X251317513>

- [20] Lochmann M, Kalesse-Los H, Schäfer M, Heinrich I, Leinweber R. Analysing wind power ramp events and improving very short-term wind power predictions by including wind speed observations. *Wind Energy*. 2023; 26(6): 573-588. <https://10.1002/we.2816>
- [21] Yao Yao He, Chuang Zhu, Chaojin Cao, A wind power ramp prediction method based on value-at-risk, *Energy Conversion and Management*, Volume 315, 2024, 118767, ISSN 0196-8904. <https://doi.org/10.1016/j.enconman.2024.118767>
- [22] Joseph Rawson, Domniki Ladopoulou, and Petros Dellaportas. Multi-task neural diffusion processes for uncertainty-quantified wind power prediction, Version Number: 1. <https://arxiv.org/abs/2510.03419>
- [23] X. Lu, J. Qiu, Y. Yang, C. Zhang, J. Lin and S. An, "Large Language Model-Based Bidding Behavior Agent and Market Sentiment Agent-Assisted Electricity Price Prediction," in *IEEE Transactions on Energy Markets, Policy and Regulation*, vol. 3, no. 2, pp. 223-235, June 2025. <https://doi.org/10.1109/TEMPR.2024.3518624>
- [24] Alharbi, F.R.; Csala, D. A Seasonal Autoregressive Integrated Moving Average with Exogenous Factors (SARIMAX) Forecasting Model-Based Time Series Approach. *Inventions* 2022, 7, 94. <https://doi.org/10.3390/inventions7040094>
- [25] Grothe, O.; Kächele, F.; Watermeyer, M. Analyzing Europe's Biggest Offshore Wind Farms: A Data Set with 40 Years of Hourly Wind Speeds and Electricity Production. *Energies* 2022, 15, 1700. <https://doi.org/10.3390/en15051700>